SUMMARY REPORT

CONTRACT NO. NASW-1404

HIGH-TEMPERATURE LIQUID-MERCURY CATHODES FOR ION THRUSTERS

HUGHES

HUGHES AIRCRAFT COMPANY

W.O. ECKHARDT, K.W. ARNOLD, G.HAGEN
J.HYMAN, JR., J.A.SNYDER, AND R.C. KNECHTLI

1 JUNE 1966 through 31 JULY 1967

HUGHES RESEARCH LABORATORIES • MALIBU

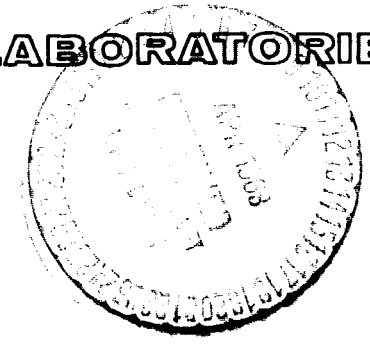

HIGH-TEMPERATURE LM CATHODES FOR ION THRUSTERS

Summary Report

1 June 1966 through 31 July 1967

CONTRACT NASW-1404

prepared for

NATIONAL AERONAUTICS AND SPACE ADMINISTRATION

by

W. O. Eckhardt, K. W. Arnold, G. Hagen, J. Hyman, Jr.,
J. A. Snyder, and R. C. Knechtli

Technical Management
NASA-Headquarters
Washington, D. C.
G. W. Pfannebecker

HUGHES RESEARCH LABORATORIES
A Division of Hughes Aircraft Company
3011 Malibu Canyon Road
Malibu, California

TABLE OF CONTENTS

LIST OF ILLUSTRATIONS

ABSTRACT

Liquid-Metal (LM) cathodes of annular geometry have been satisfactorily operated in electron-bombardment thrusters at temperatures up to 300°C. Analysis is presented which demonstrates that this temperature is sufficiently high to permit rejection of waste discharge heat from the thruster shell at a temperature of 200°C or more. This capability provides an independence of the cathode from the thermal constraints of actual thruster operation in space, whether these arise from peripheral clustering or from solar incidence. All the demonstrated advantages of low-temperature LM cathodes (practically unlimited life, adjustable electron-to-atom emission ratio, etc.) are still available at these elevated temperatures. We have demonstrated source energies per ion as low as 400 eV/ion (note that there is no heater power with the LM cathode) at 87% mass utilization in a 20-cm thruster with a cathode temperature of 250°C (at 300°C:443 eV/ion at 84% mass utilization). Furthermore, stable LM cathode operation has been demonstrated in the neutralizer current range with very attractive electron-to-atom emission ratios (50 and better) and power expenditures (≈ 20 eV/electron), at temperatures close to the equilibrium temperature of a neutralizer which is cooled only by radiation from its face. Finally, diagnostic experiments performed on operating thrusters have led to a better understanding of the thruster discharge which can now be used as the basis for further performance improvements.

I. INTRODUCTION AND SUMMARY

Shortly after the initial development of the Kaufman mercury electron-bombardment thruster,[1] it appeared that some distinct advantages were to be gained by replacing the thermionic cathode of the original thruster with a mercury surface electron source, or LM cathode.* Apart from the convenience of using the cathode also as the source of propellant vapor, the problem of cathode surface degradation by ion sputtering is eliminated in the LM cathode since the sputtered surface is mercury, rather than an oxide coating of a thermionic cathode. This sputtering of an LM cathode merely adds a small amount to the natural efflux of atoms evaporating from the mercury surface which is continually replenished.

The feasibility of system life in excess of 10^4 hours was demonstrated at Hughes Research Laboratories when a 20-cm thruster equipped with a circular LM cathode was successfully tested for an accumulated 4,000 hours.[4] Following this test no erosion of the molybdenum cathode structure was evident, and no degradation of the cathode performance occurred. Furthermore, remarkable time invariance of cathode and thruster characteristics was demonstrated, as well as insensitivity to environmental conditions.

For optimum performance, the electron-to-atom emission ratio K_e/K_a must be kept at a value which depends on the detailed discharge chamber and magnetic field configuration. The best results to date have been obtained for $K_e/K_a \cong 10$ to 15. For a given cathode geometry and discharge current, a maximum mercury surface temperature T_{Hg} exists for which a given value of K_e/K_a can be maintained; if this temperature is exceeded, either the rate of mercury evaporation becomes excessive and K_e/K_a must be made smaller than the desired value, or the mercury surface retracts into the throat of the nozzle and the discharge extinguishes.

There are two reasons for desiring a relatively high mercury surface temperature T_{Hg}: (1) to be able to reject the cathode heat through the thruster shelf (even in a dense array of thrusters) and (2) to accommodate the temperature rise resulting from exposure to solar radiation. The thermal load $P_{K,th}$ which the cathode receives from ion bombardment must be conducted by the thruster end plate to

*For brevity, the gravity-independent, force-fed liquid metal cathode invented[2] and developed[3] at HRL will be referred to as the Liquid Metal, or LM cathode. In this report the specific liquid metal is mercury.

the thruster shell, and rejected there. At the same time the fraction of the anode heat flux which is not radiated in the direction of the beam is also rejected by the shell. The thruster shell temperature which is required to radiate this heat (together with the thermal resistance of the heat conducting path from the mercury surface at the cathode to the shell and with the thermal load $P_{K,th}$) thus determines the minimum mercury surface temperature which must be made compatible with $K_e/K_a \geq 10$, in order that thruster performance is not impaired.

It has been found that, in a peripheral array of 20-cm diameter thrusters, $P_{K,th}$ can be radiated by the thruster shells provided the mercury surface temperature is 300°C. This result is obtained under the realistic conditions that the specific heat loading of the cathode does not exceed 7.5 WA^{-1}, and that heat shielding between the anode and the thruster shell be 90% effective. For a 20-cm diameter thruster, it is shown that under the above conditions and for an over-all weight of about 8 lb, the shell can operate at 175°C when the beam current is 600 mA and $K_e/K_a = 12$. At a specific impulse of 4000 sec, $\eta_m = 90\%$, and a thruster power efficiency of 82% (450 eV/ion), the corresponding weight-to-power ratio would be 5.3 lb/kW.

Because a mercury surface temperature of $T_{Hg} = 300^{\circ}C$ is substantially above the temperatures of conventional mercury pool devices, it was necessary to develop high-temperature LM cathodes. The work conducted under the subject contract has stressed the use of an annular rather than circular geometry for the pool-keeping structure (Fig. 1). The ratio of the mercury pool perimeter to the discharge current is much greater for the former geometry than for the latter, so that the annular cathode can more easily dissipate the thermal load,[5] especially at high beam currents. Typical data show that for a circular cathode the temperature differential between the pool and a thermocouple 4 mm away might be as great as 98°C, whereas with the same $P_{K,th}$ and an annular pool geometry the temperature differential is reduced to 21°C.

The results obtained have led to the successful development of an annular LM cathode design, capable of operating at the required mercury surface temperature of 300°C, with $K_e/K_a \geq 10$ and a specific heat load on the order of 7.5 WA^{-1}. Furthermore, efficient thruster operation has been demonstrated with this cathode (total ion source power expenditure of $\sim$ 400 eV/ion at a mass utilization efficiency $\eta_m > 80\%$). Thus the requirements for operation in a peripheral cluster of thrusters (and, a fortiori, for a single thruster) have been satisfied.

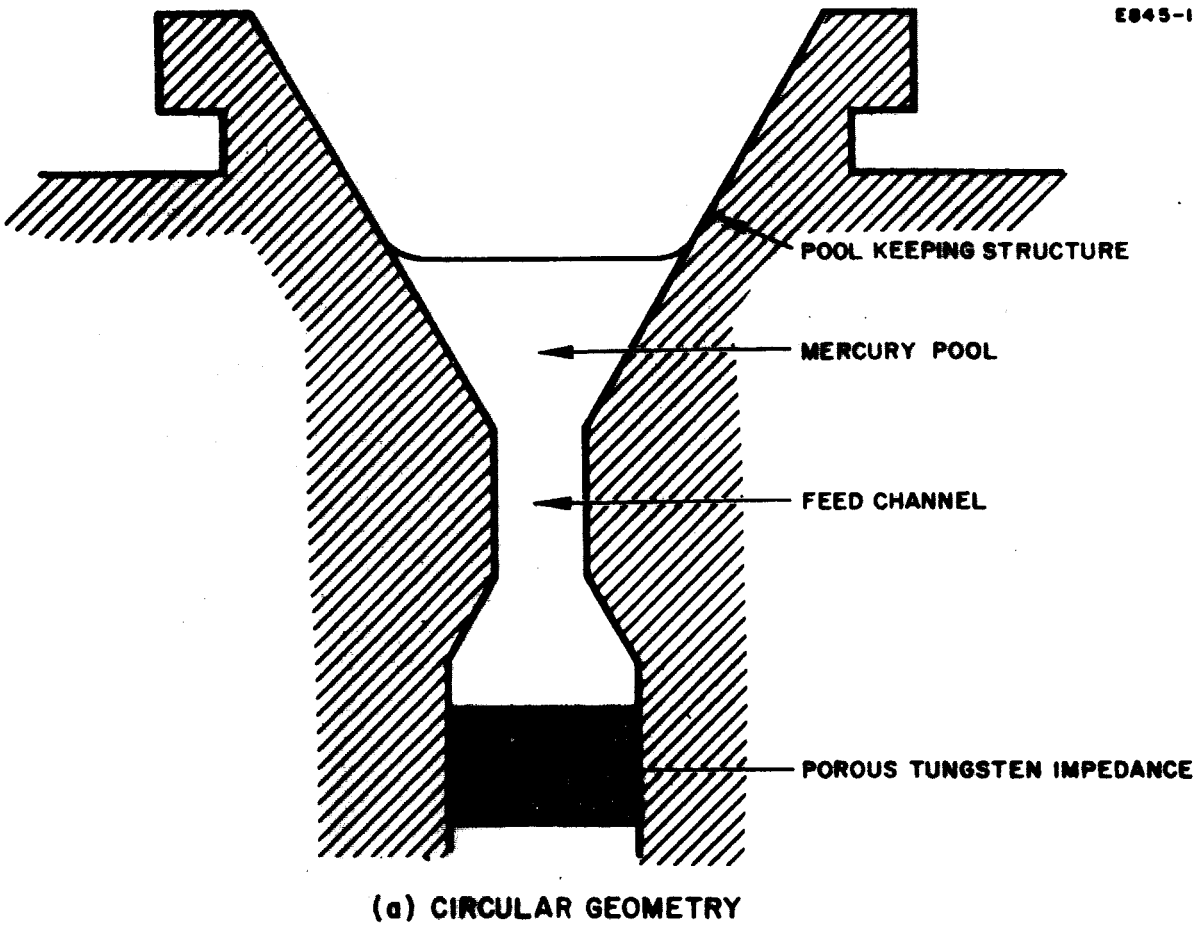

Fig. 1. Circular and annular cathode geometries.

Section III-B describes work performed on an LM neutralizer cathode. Replacement of a mechanical by an electrical igniter showed that in earlier experiments the predominant mercury loss was, as speculated, by igniter splashing rather than by evaporation. As a consequence, stable LM cathode operation in the neutralizer current range was demonstrated at good electron-to-atom emission ratios (> 50) for periods up to several hours, at temperatures close to the equilibrium value at which cooling occurs by radiation from the neutralizer face, and with power expenditures of only ≈ 20 eV/electron.

Diagnostic experiments, using both plasma probes within the discharge chamber of an operating thruster and baffles with movable apertures or apertures of variable size, have improved considerably our understanding of the discharge mechanism. The significance of these findings is that they point out the possibility of independently affecting the admission of electrons and neutral atoms into the discharge chamber, using improved versions of our discharge chamber baffles. This should lead to further substantial increases in thruster efficiency.

II. ANALYSIS OF THERMAL DESIGN REQUIREMENTS

A. Introduction

Operation of the LM cathode at high temperatures (250 to 300°C) is achieved by shrinking the exposed mercury surface to a small size in order to reduce the evaporation of mercury and to keep the electron-to-atom ratio at the cathode, K_e/K_a, at the desired level (from 10 to 20). The thermal design requirements for the high-temperature LM cathode were considered earlier,[5] and the advantages of annular over circular cathode geometry in heat conduction for the mercury pool were clearly demonstrated. The analysis contained here is somewhat more comprehensive, and includes rejection of heat from the thruster shell.

B. Cathode Parameters

This analysis will consider only circular and annular LM cathode geometries, although it is expected that the thermal properties of a high temperature rectangular slit cathode would be similar to those of an annular cathode. The circular cathode is shown in Fig. 2, while Fig. 3 is a section of an annular cathode, with mean annular radius $\bar{r}$ and width of exposed mercury surface Δr. Other parameters are the beam current I_B; the mass utilization η_m; the cathode current I_K; the flux density L_a of the evaporating mercury atoms; the area of the exposed mercury surface A_K at the cathode; the temperature of the mercury T_{Hg}; the heat conductivity k_{th} of the cathode material; and the ratio $V_{K,th}$ of the thermal power delivered to the cathode $P_{K,th}$ to the cathode current I_K.

Assuming that evaporation is the predominant loss of mercury from the cathode, and that back scattering can be neglected, then

$$L_a = \frac{1}{4} n \bar{c},$$

where n is the equilibrium number density in saturated mercury vapor equivalent to temperature T_{Hg} and $\bar{c}$ is the mean vapor velocity. As a consequence, we also have

$$L_a = \frac{p_{Hg}(T_{Hg})}{(2\pi m_{Hg} k T_{Hg})^{1/2}},$$

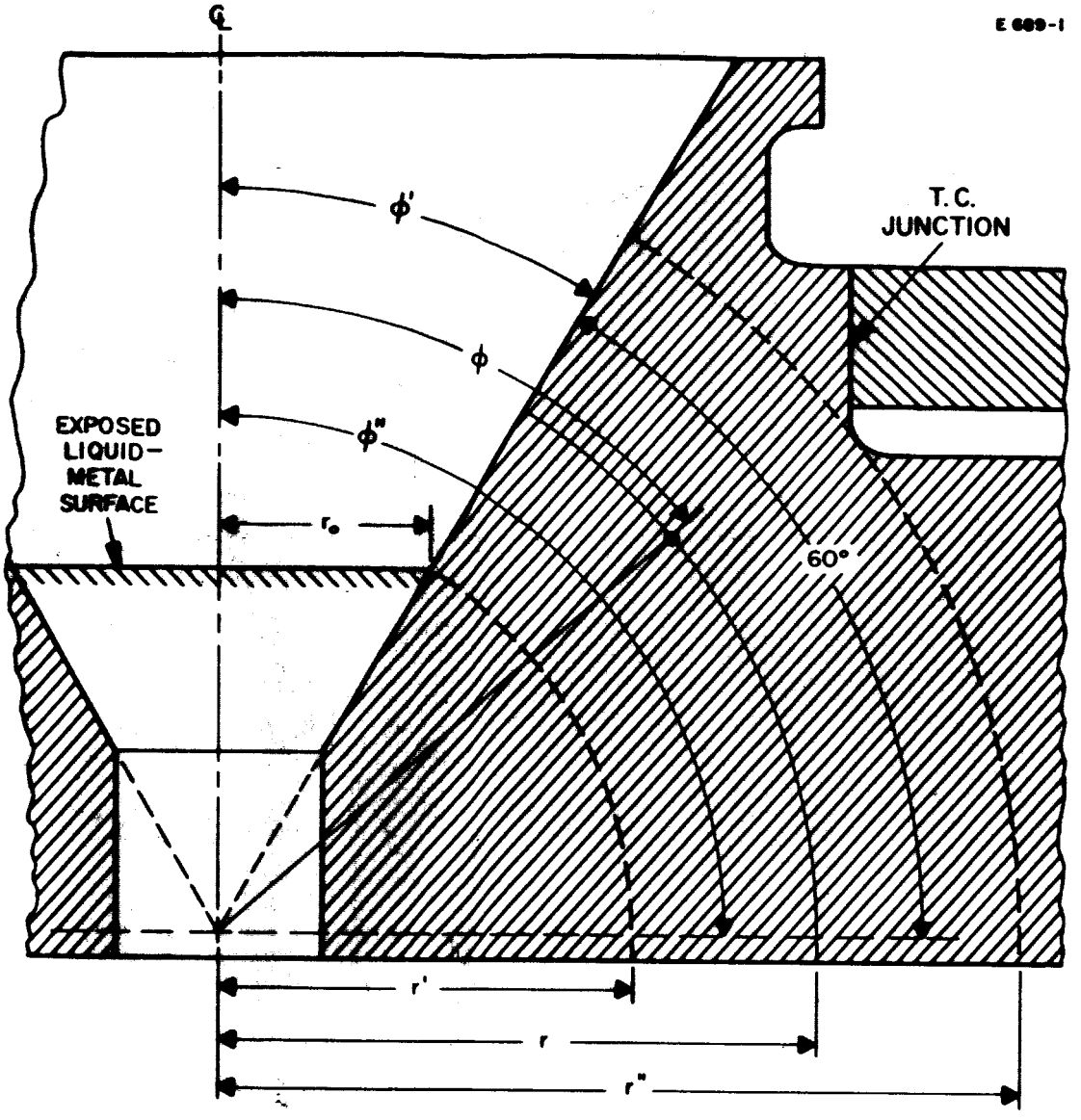

Fig. 2 . Schematic cross section of circular LM cathode design (not to scale).

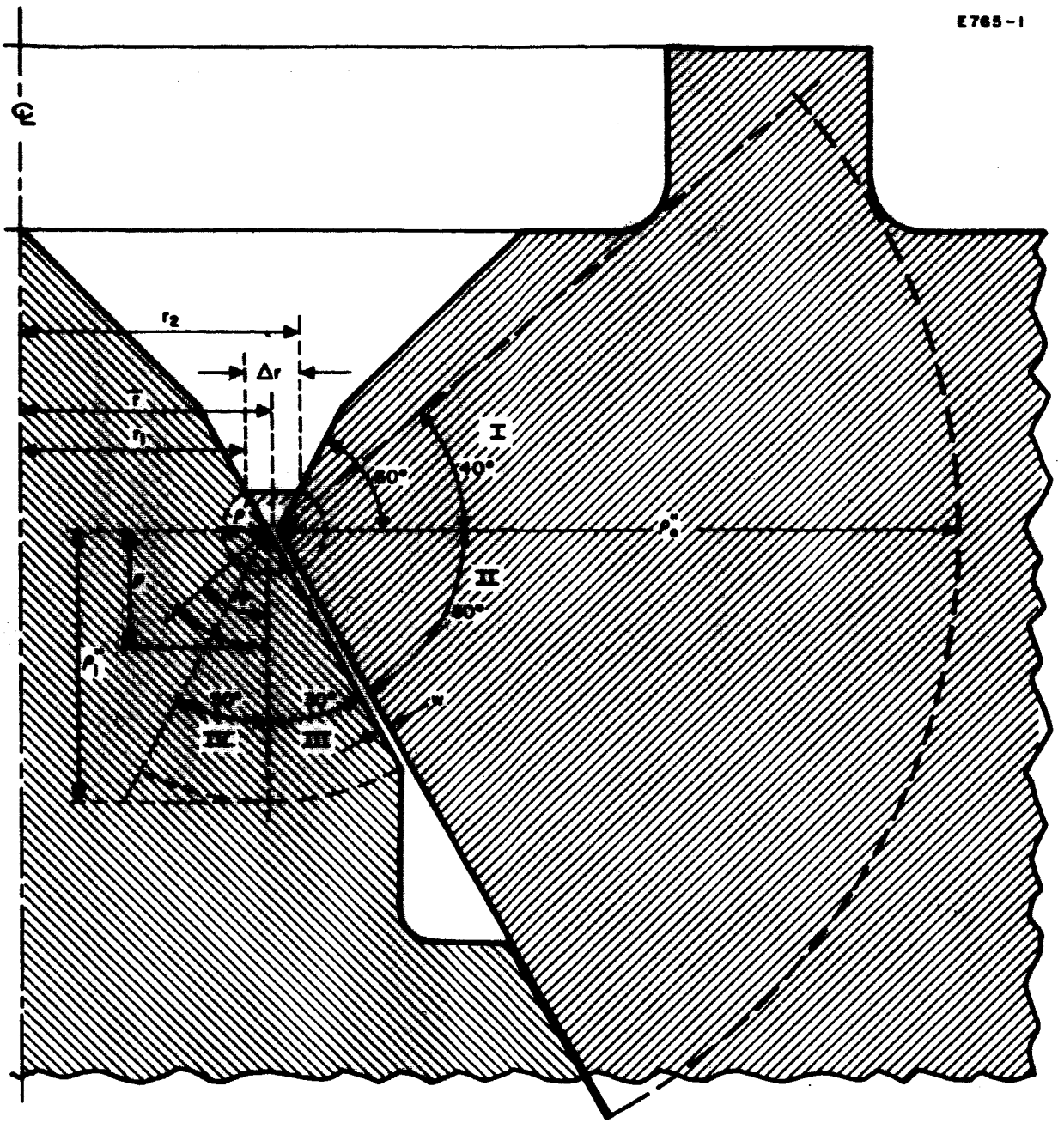

Fig. 3. Schematic cross section of annular LM cathode design (not to scale).

where $p_{Hg}(T_{Hg})$ is the saturated vapor pressure of mercury, m_{Hg} is the atomic mass of Hg and k is Boltzmann's constant.

The total number of atoms evaporated per second is then

$$K_a = L_a A_K = \frac{\pi r^2 p_{Hg}}{(2\pi m_{Hg} k T_{Hg})^{1/2}} \quad \text{for the circular cathode}$$

and

$$K_a = \frac{2\pi \bar{r} \Delta r \, p_{Hg}}{(2\pi m_{Hg} k T_{Hg})^{1/2}} \quad \text{for the annular cathode.}$$

Figure 4 shows p_{Hg}, L_a and the ratio I_B/A_K as functions of T_{Hg}, the latter for values of η_m = 100, 90, and 80%.

The range of T_{Hg} between 200 and 350°C (473 to 623°K) is particularly interesting. In Fig. 5 the relationship

$$A_K = I_K/(eL_a K_e/K_a) \quad \text{(where } e \text{ is the electronic charge)}$$

is plotted for various temperatures T_{Hg} and values of the electron-to-atom emission ratio K_e/K_a. For example with I_B = 0.250 A, η_m = 85% and T_{Hg} = 300°C, A_K = 7.5 x 10^{-5} cm^2, and I_K = 3.16 A with K_e/K_a = 10.

C. Cathode Temperature Measurements

Because of the small area of the mercury surface and the relatively low thermal conductivity of mercury (about 10 times less than molybdenum), it is not possible to measure the mercury temperature directly with a thermocouple. Instead, the junction was placed a short distance from the pool and the temperature difference $T_{Hg} - T_K$ was estimated. This was done in the case of the circular cathode by assuming concentric spherical isotherms (Fig. 2) between the mercury pool and the thermocouple junction.

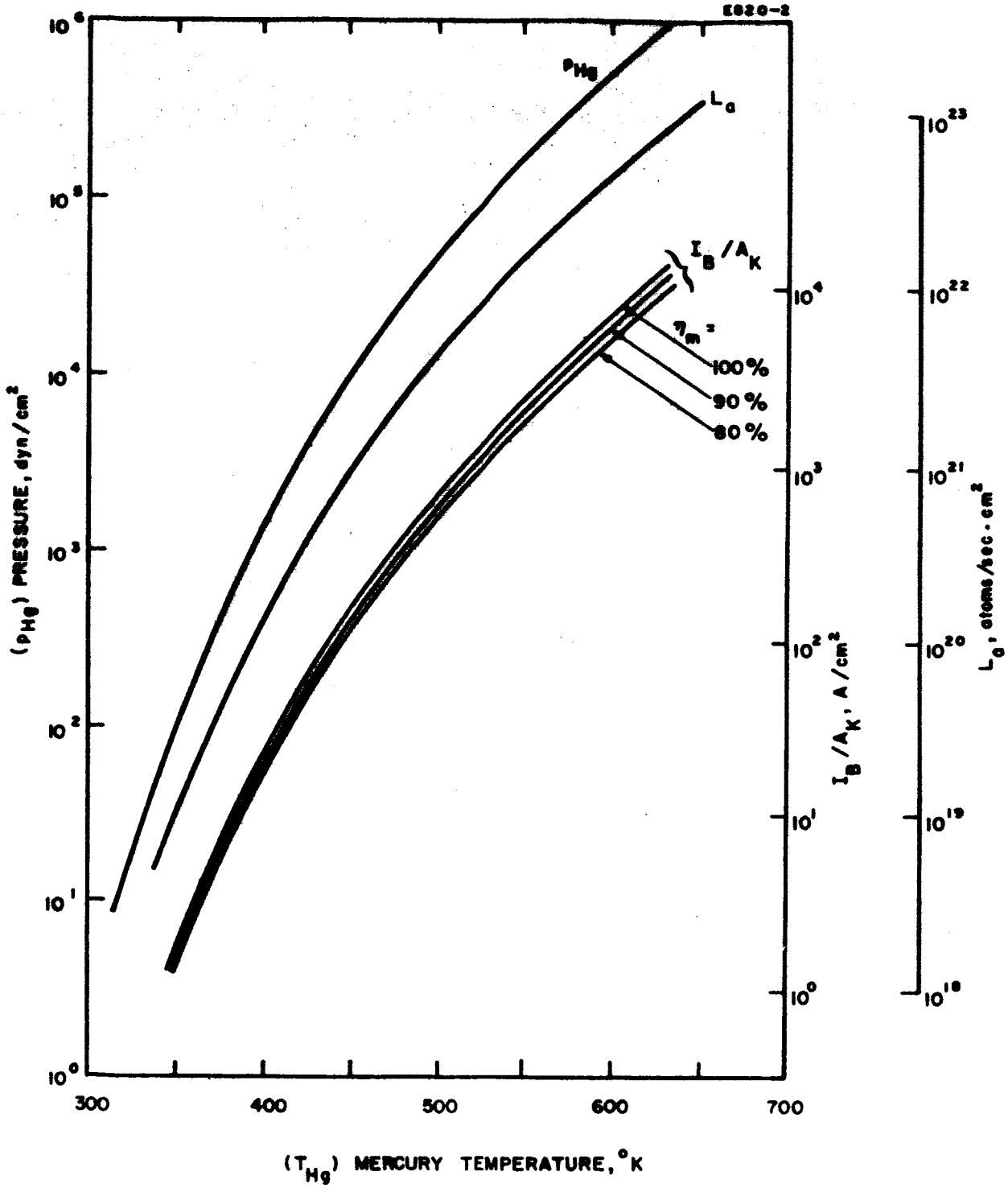

Fig. 4. Saturated vapor pressure p_{Hg}, evaporation rate and ratio I_B/A_K as a function of mercury temperature.

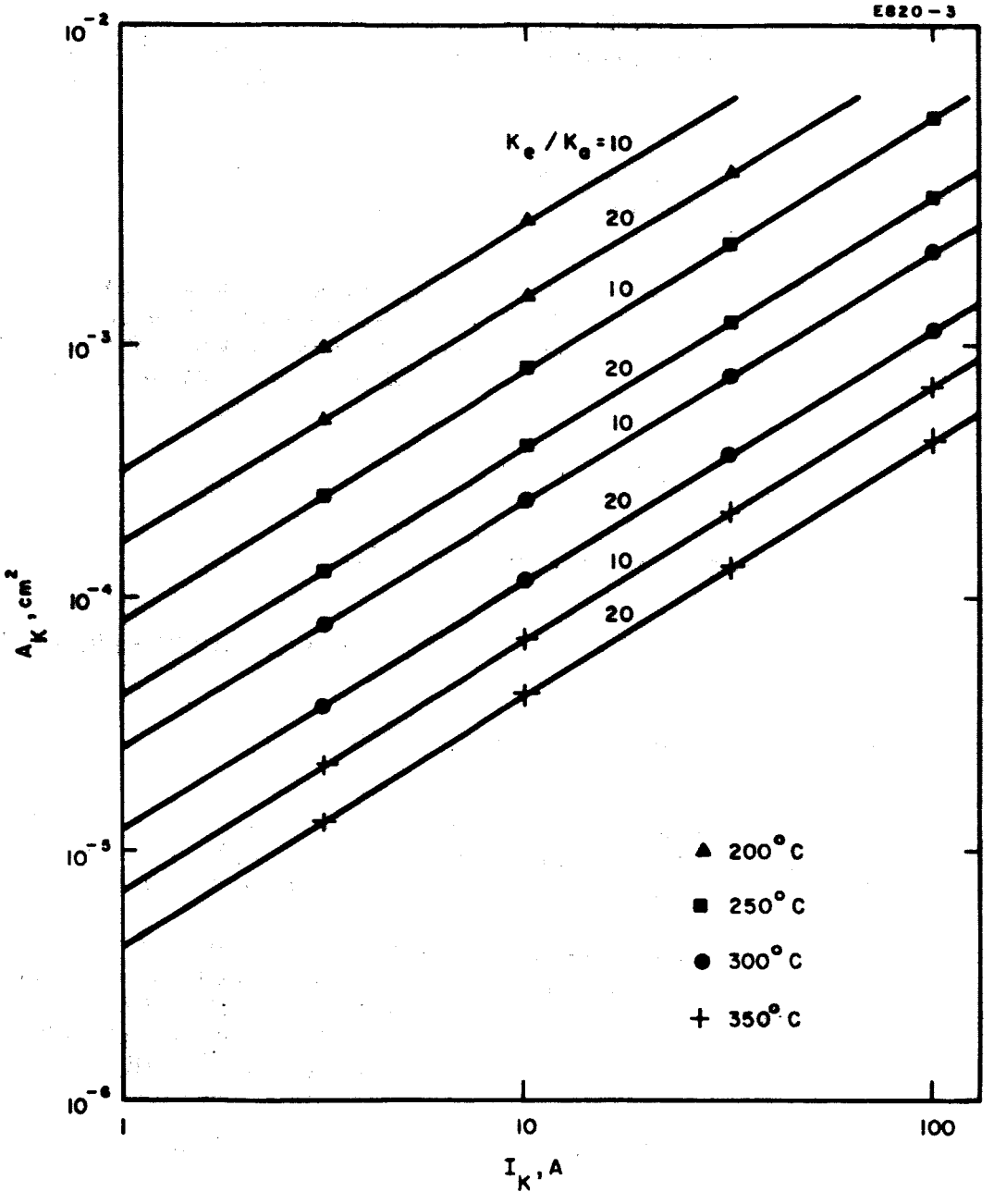

Fig. 5. A_K as a function of I_K for various T_{Hg} and K_e/K_a values.

With this assumption, the thermal resistance $R_{K,th}$ of a circular cathode between pool and thermocouple location is given by the following expression*:

$$R_{K,th} = \frac{1}{2\pi k_{th}(\cos\phi' - \cos\phi'')} \cdot \frac{r'' - r'}{r' r''} .$$

Here, k_{th} is the thermal conductivity of the pool-keeping structure material, while the quantities ϕ', ϕ'', r', and r'' are defined by Fig. 2. For a typical molybdenum circular cathode such as that of the life-test thruster, we have

$$k_{Mo} = 1.46\ W \cdot cm^{-1} \cdot (^{o}K)^{-1} ,$$

$$\phi' = 30^{o},\ \phi'' = 90^{o},\ r'' = 3.8\ mm .$$

We note (see Fig. 2) that

$$r' = r_o/\sin\phi' = 2\,r_o ,$$

so that the thermal resistance varies only with the size of the circular mercury pool of area $A_K = \pi r_o^2$. This variation of $R_{K,th}$ with A_K is exhibited in Fig. 6.

In the annular case the cathode environs were divided into regions I to IV, as shown on Fig. 3, and concentric toroidal isotherms were assumed within each region. Now the thermal resistance of one region between two toroidal isotherms of major radius $\bar{r}$ and minor radii ρ' and ρ'' is

$$R_{K,th}^{(n)} = \frac{1}{2\pi k_{th} b} \ln \frac{\rho''(c\rho' + b)}{\rho'(c\rho'' + b)} ,\quad n = I \ldots IV,$$

where $b = \bar{r}(\phi'' - \phi')$ and $c = \cos\phi' - \cos\phi''$. For the specific geometry of Fig. 3, ρ' is also equal to Δr, and because $\bar{r} >> \Delta r$,

$$R_{K,th} \approx \frac{1}{2\pi k_{th} b} \ln \frac{\rho'' b}{\Delta r(c\rho'' + b)} .$$

*A complete description of the analysis for both the circular and the annular case is given in Quarterly Progress Report No. 1, Contract No. NASW-1404.

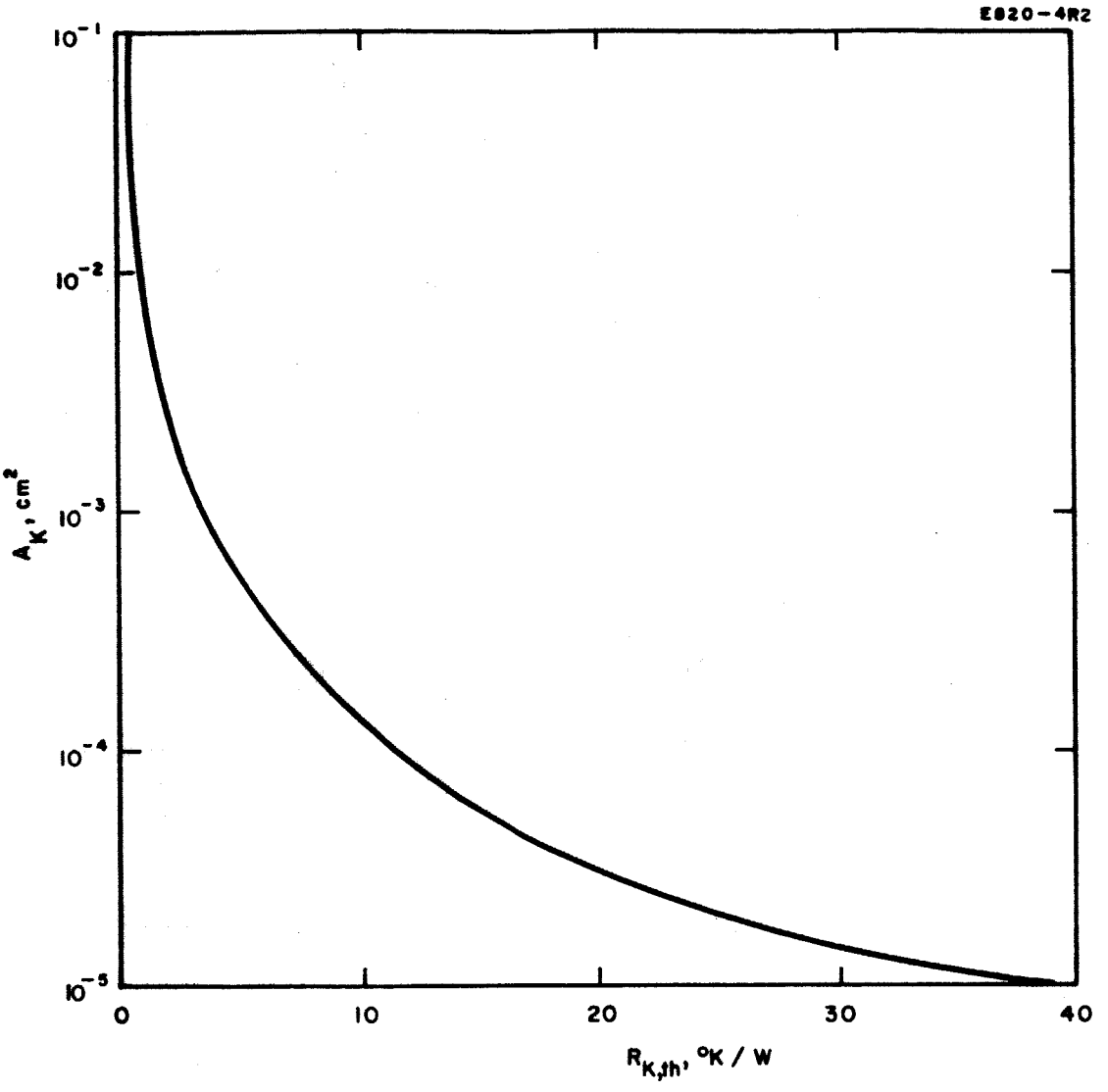

Fig. 6. Circular cathode thermal resistance as a function of mercury surface area.

The total thermal resistance of an annular cathode between pool and thermocouple location becomes

$$R_{K,\,th} \approx \frac{1}{\sum_{n} 1/R_{K,\,th}^{(n)}} \quad .$$

Figures 7 through 11 show the dependence on A_K of $R_{K,\,th}^{(n)}$ (n = I ... IV) and $R_{K,\,th}$. In zones I and II, ρ'' was taken as 0.25 cm, and in zones III and IV it was taken as 0.075 cm. As $\bar{r}$ is lowered from 0.21 to 0.15 cm, the value of $R_{K,\,th}$ for a particular A_K increases. In order to minimize the temperature drop between the mercury pool and the radiating surface, a low value for $R_{K,\,th}$ is needed, leading to a large value for $\bar{r}$. In practice $\bar{r}$ is limited by the dimension Δr, which cannot conveniently be less than about 5×10^{-4} cm. In Fig. 3, $\bar{r}$ = 0.19 cm, giving $\Delta r = 5 \times 10^{-4}$ cm for $A_K = 6 \times 10^{-4}$ cm^2.

To compare the two geometries, consider a cathode operating at T_{Hg} = 250°C, with an I_B = 500 mA at η_m = 90%; then from Fig. 5, $A_K = 4.2 \times 10^{-4}$ cm^2, and with K_e/K_a = 12, I_K = 6.5 A. From Fig. 6 the thermal resistance for the circular cathode which corresponds to this A_K is 5.5° K W^{-1}, while from Fig. 11 for a representative annular cathode ($\bar{r}$ = 0.19 cm) it is 1.3°K W^{-1}. Assuming a value for $V_{K,\,th}$ of 2.5 WA^{-1} the temperature difference between the mercury pool and the thermocouple, 0.44 cm from the center line of the cathode, is 89°C for the circular and 21°C for the annular cathode.

D. Variation with Beam Current

It is also pertinent to consider the variation of the temperature difference $T_{Hg} - T_K$ with the mercury pool temperature T_{Hg} for different values of I_B.

From the relationship

$$A_K = I_B/eL_a\eta_m,$$

A_K can be determined as a function of T_{Hg}. This is independent of the geometry of A_K and is shown in Fig. 12 for three values of I_B. It can also be seen from the figure that the function is relatively insensitive to a change in η_m from 100% to 80%, so that for clarity the curves for I_B = 400 mA and 200 mA are shown for η_m = 90% only. Again choosing Cathode No. 26 (mean annular radius 0.19 cm) as representative of the annular configuration, combination of Fig. 12 with Figs. 6 and 11 then gives the data for Figs. 13 and 14.

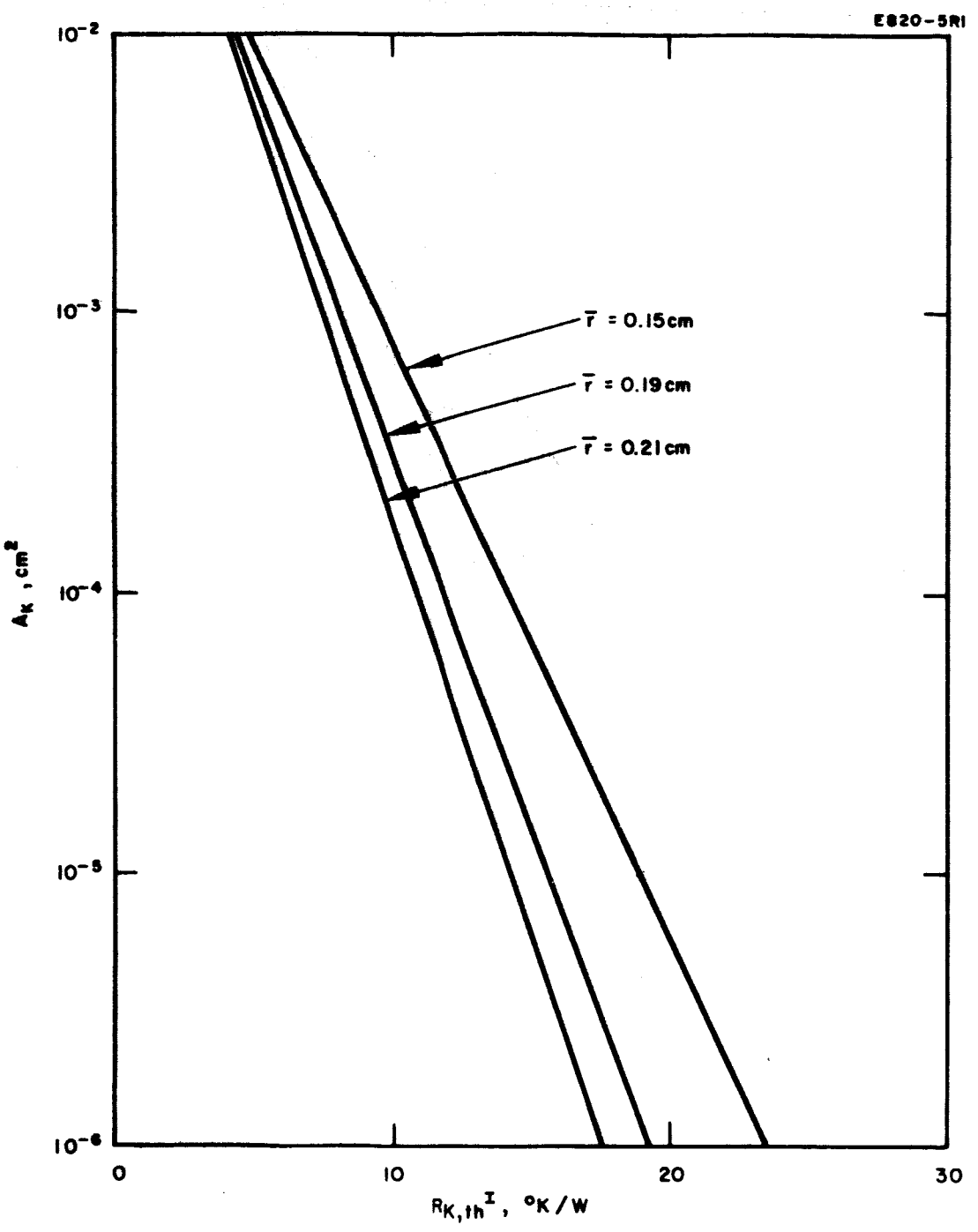

Fig. 7. Thermal resistance in annular cathode region I as a function of mercury surface area.

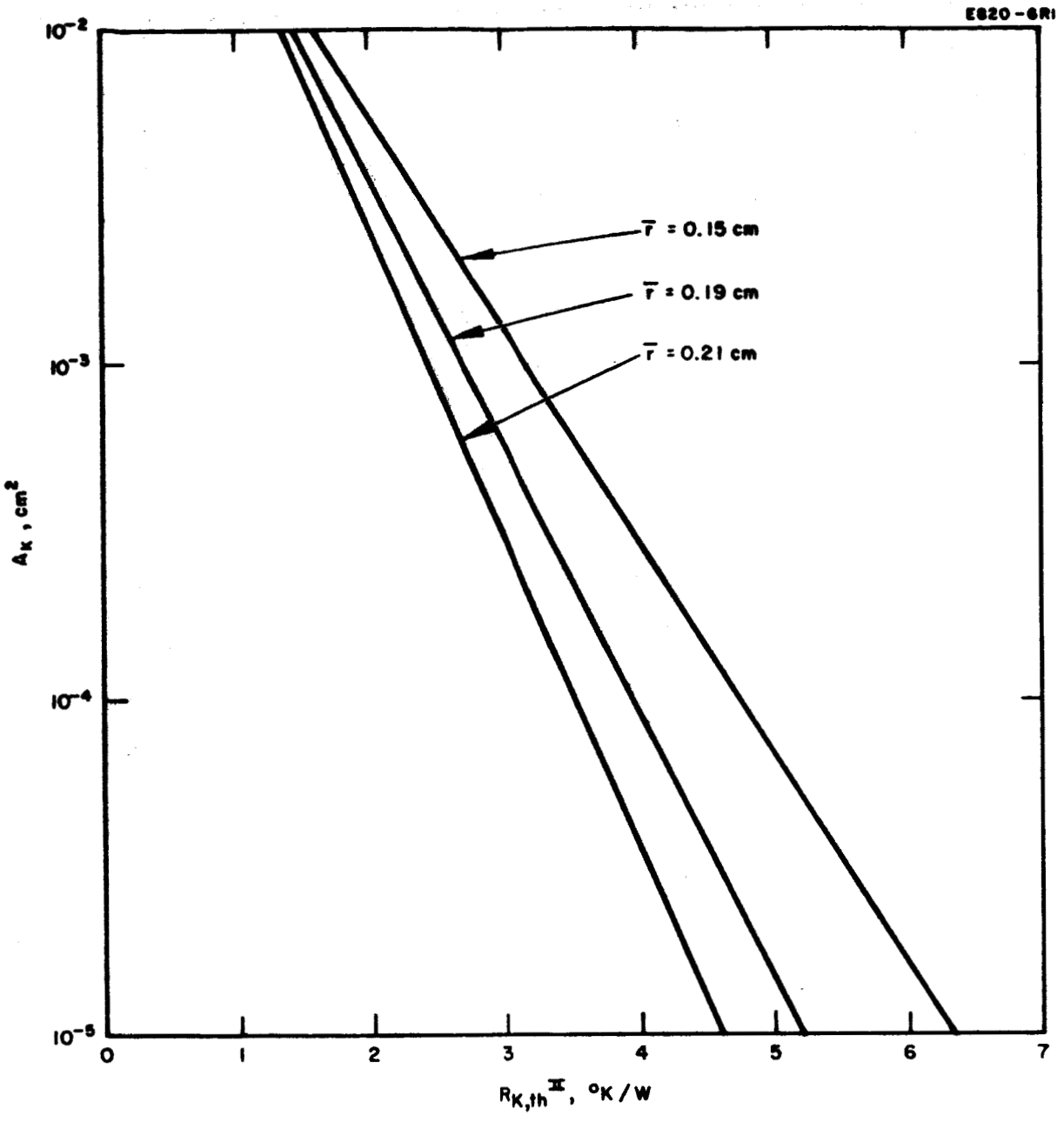

Fig. 8. Thermal resistance in annular cathode region II as a function of mercury surface area.

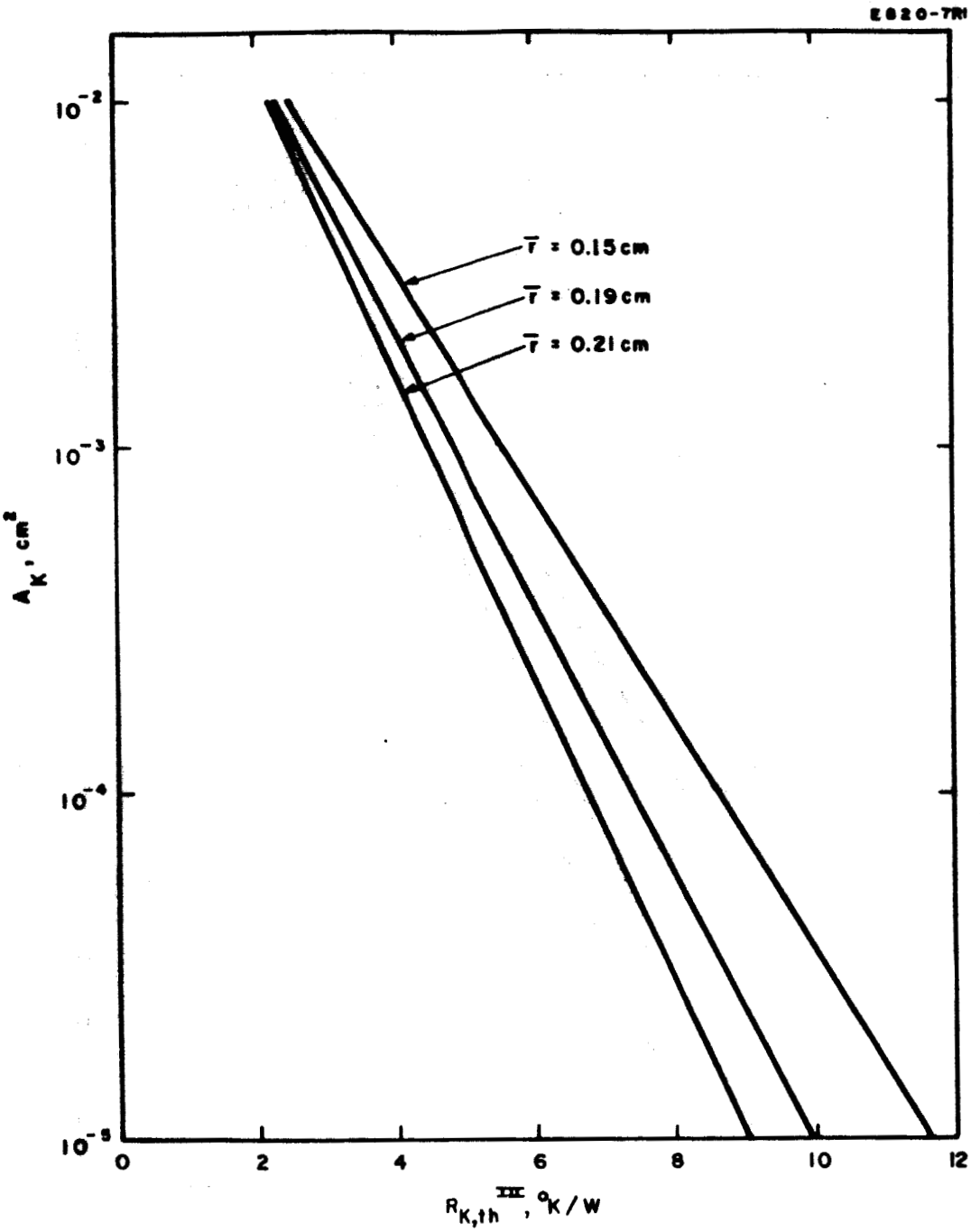

Fig. 9. Thermal resistance in annular cathode region III as a function of mercury surface area.

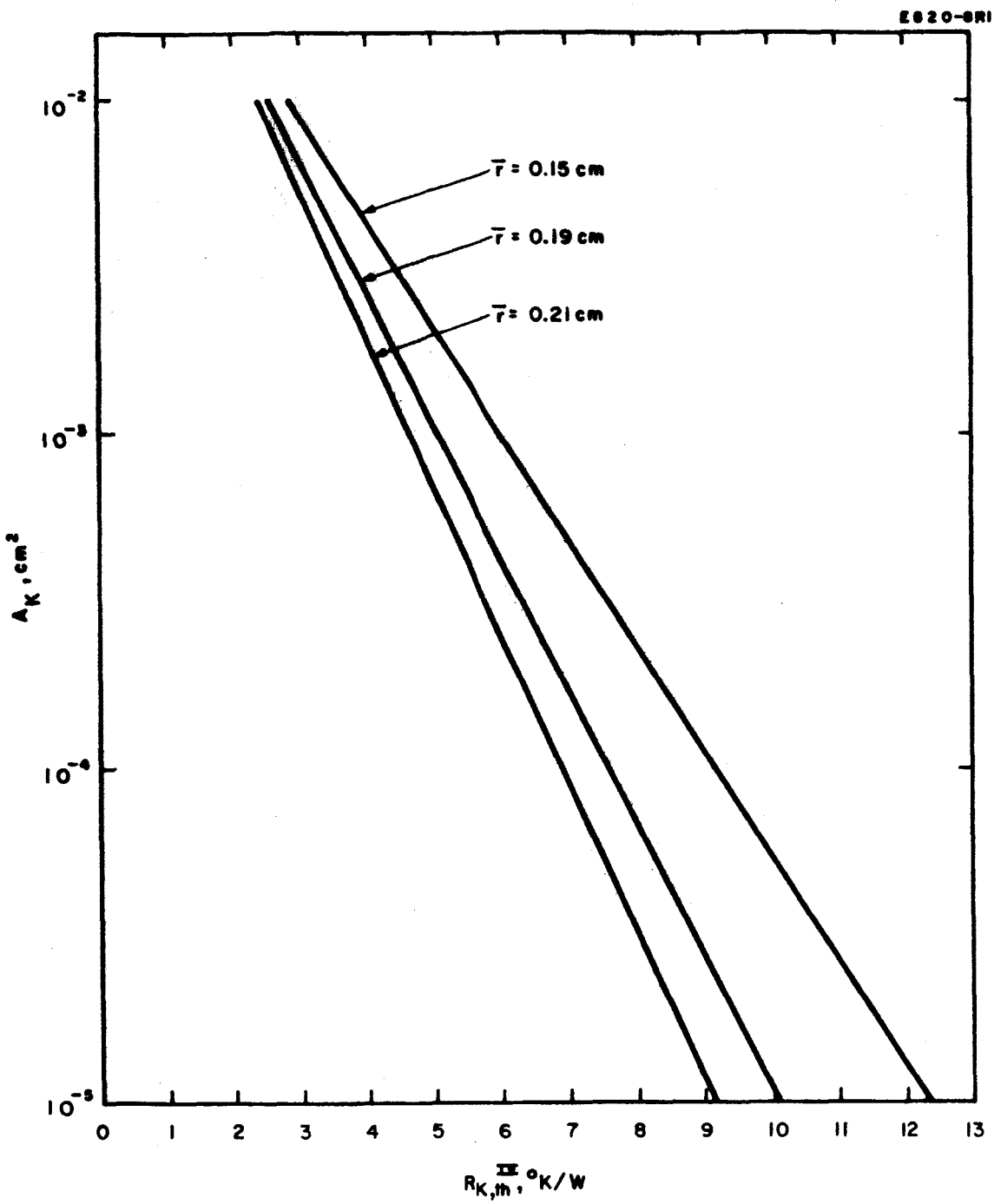

Fig. 10. Thermal resistance in annular cathode region IV as a function of mercury surface area.

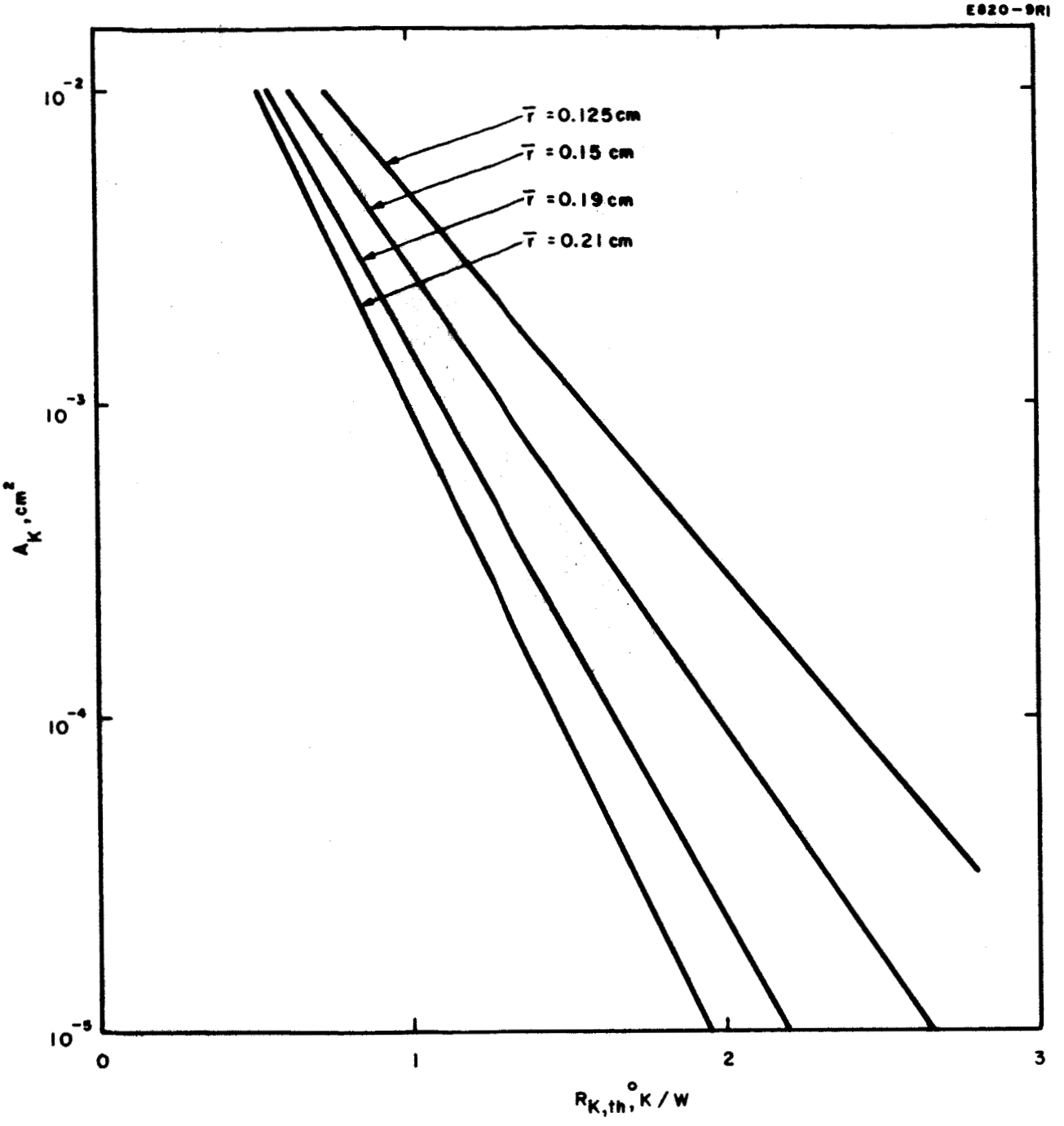

Fig. 11. Total thermal resistance of annular cathode as a function of mercury surface area.

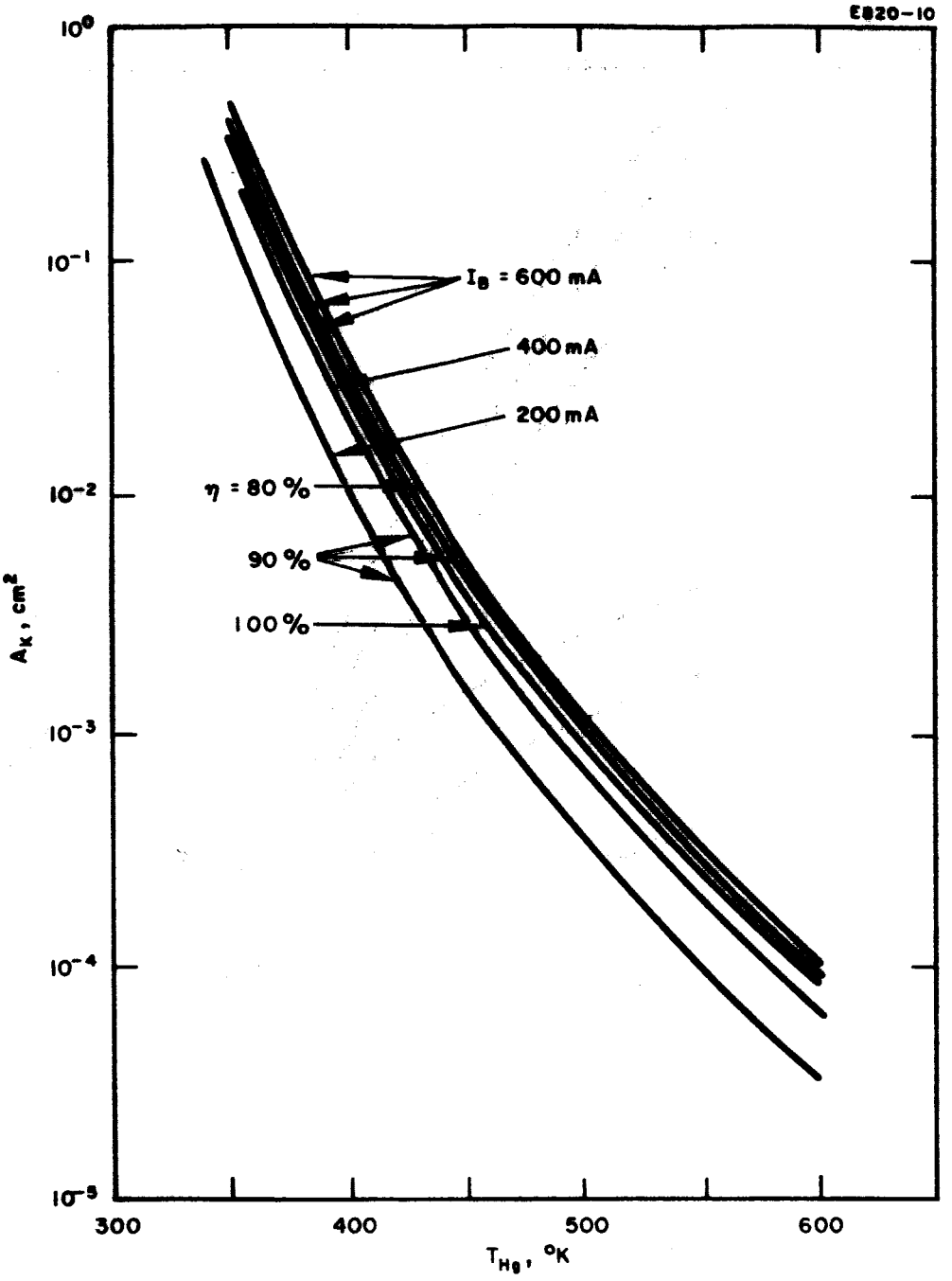

Fig. 12. Mercury surface area A_K as a function of T_{Hg} for different values of I_B and η_m.

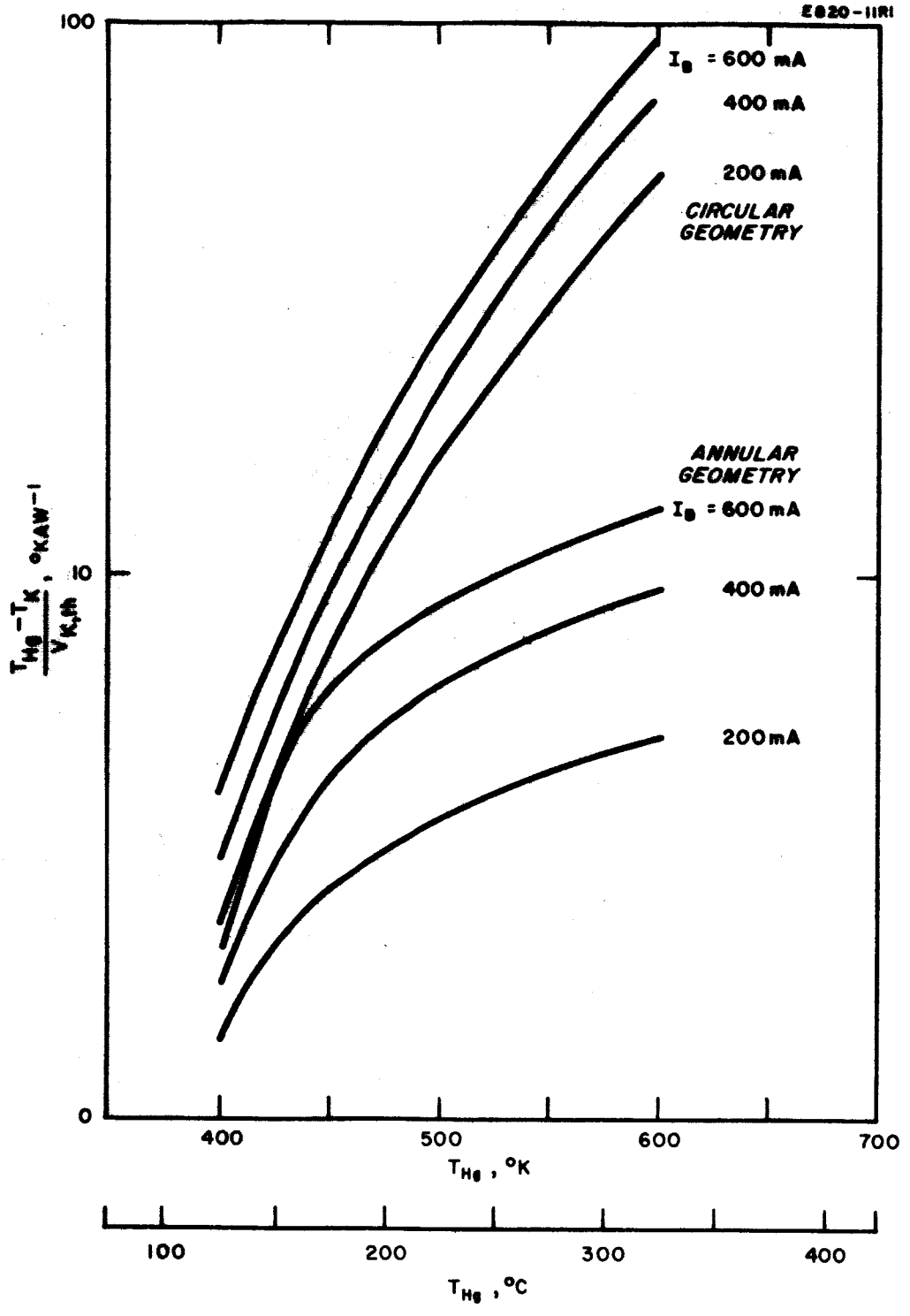

Fig. 13. Temperature difference $T_{Hg} - T_K$ per unit cathode specific heat loading $V_{K,th}$ as a function of T_{Hg}. (η_m = 90%, K_e/K_a = 12.)

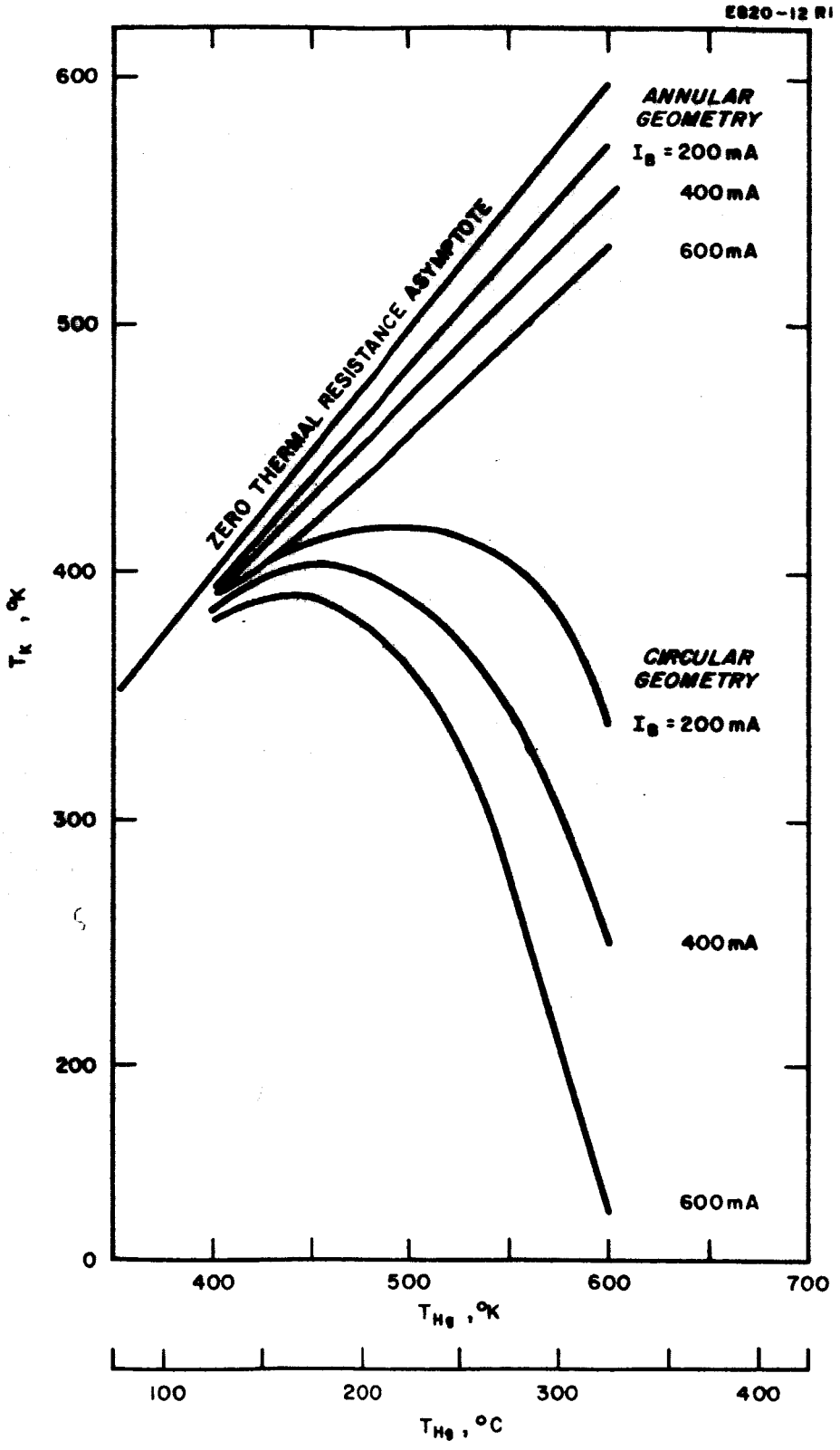

Fig. 14. T_K as a function of T_{Hg} for annular and circular cathode geometries ($V_{K,th} = 5\ WA^{-1}$, $\eta_m = 90\%$, $K_e/K_a = 12$).

Figure 13 shows the relationship between T_{Hg} and the temperature difference $T_{Hg}-T_K$ for unit cathode specific heat loading $V_{K,th}$. In Figs. 13 and 14 it has been assumed that η_m = 90% and the electron-to-atom ratio at the cathode, K_e/K_a = 12. The I_K values equivalent to I_B = 600, 400, and 200 mA are then 8.0, 5.33, and 2.66 A, respectively. For a particular value of I_B the curves for circular and annular cathode geometry merge at low values of T_{Hg}, but for practical temperatures (T_{Hg} from 130° to 300°C), annular geometry produces much smaller values of $(T_{Hg}-T_K)/V_{K,th}$ than does a circular geometry.

This is shown more clearly in Fig. 14, where the temperature T_K at the thermocouple junction has been drawn as a function of the pool temperature T_{Hg} for different I_B, assuming a constant value for $V_{K,th}$ of 5.0 WA^{-1} throughout, and again K_e/K_a = 12 with η_m = 90%. The ideal case — that of zero cathode thermal resistance — is given by the asymptote, and the relative merit of a cathode geometry can be judged by how closely the curves for a given I_B approach the asymptote. Again the curves for annular and circular cathode geometry merge at low T_{Hg}, but only those curves for annular geometry have any similarity with the asymptote for T_{Hg} > 150°C (i.e., for useful values of T_{Hg}). In fact, for this temperature regime the curves for the circular cathode depart strongly from the asymptote.

It will be shown later that the main thermal resistance opposing the flow of $P_{K,th}$ occurs between the pool and the thermocouple junction; this means that T_K relates closely to the thruster shell temperature, which should be high to aid in heat rejection. Figure 14 then shows the relative advantages of using annular rather than circular cathode geometry and clearly demonstrates that heat rejection is always accomplished with a lower temperature difference when annular rather than circular geometry is used.

E. The Outer Regions of the Cathode Matrix

The body of the cathode between the thermocouple junction and the radiating surface (thruster shell) is sketched in Fig. 15. To estimate the heat flow to the radiating edge C, it can be assumed that the isothermal surface through the thermocouple junction A is hemispherical, and that all other such surfaces are hemispherical as the radius y is increased to a distance equal to the thickness z_1 of the cathode matrix (point B). From B to C the isothermals can be thought of as being concentric cylinders.

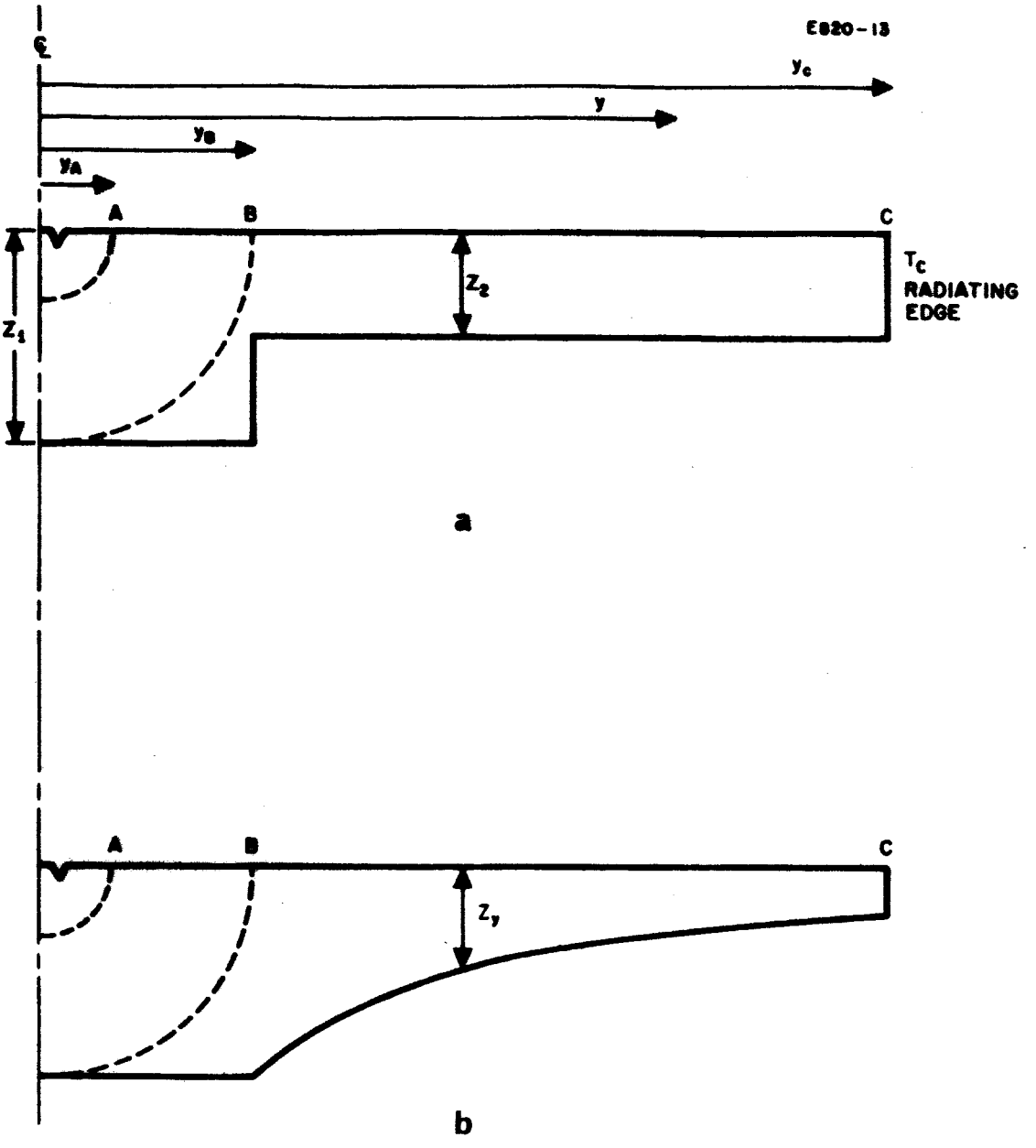

Fig. 15. Sketch of cathode outer regions.

Between A and B, the thermal resistance is

$$R_{th}^{AB} = \frac{1}{2\pi k_{th}} \frac{y_B - y_A}{y_A y_B} ,$$

which becomes

$$R_{th}^{AB} = \frac{z_1 - 0.44}{0.88 \pi k_{th} z_1} ,$$

noting that $y_B = z_1$, and taking point A to be about 0.44 cm from the center line. Figure 16 shows the ΔT between points A and B as a function of the power input to the cathode for some practical values of z_1, assuming the material to be molybdenum.

From B to the outer edge the thruster end plate may well be aluminum, with $k_{th} = 2.3$ W/°K-cm and a density of 2.7 g/cm^3. If the thickness of the cathode plate (z_2) remains constant (Fig. 15(a)) from B to C, the thermal resistance is

$$R_{th}^{BC} = \frac{1}{2\pi k_{th} z_2} \ln y_c/y_B = \frac{1}{2\pi k_{th} z_2} \cdot \ln y_c/z_1 .$$

For over-all weight reduction, $z_2 < z_1$ seems likely. Alternatively, the thickness z_2 can be made a function of y (Fig. 15(b)), and if this is such that yz = constant, the thermal resistance becomes merely

$$R_{th}^{BC} = \frac{y_c - z_1}{2\pi k_{th} z_1^2} .$$

Figures 17 and 18 show the temperature difference between B and C as a function of the power input, for various geometries.

The over-all temperature difference between the mercury pool and the radiating surface can also be plotted as a function of the weight of the cathode and end plate structure. Figure 19 shows this for a number of geometries, and shows that a good compromise between weight and heat conduction can be effected when $z_1 = 1$ cm and z_2 lies between 0.2 and 0.5 cm.

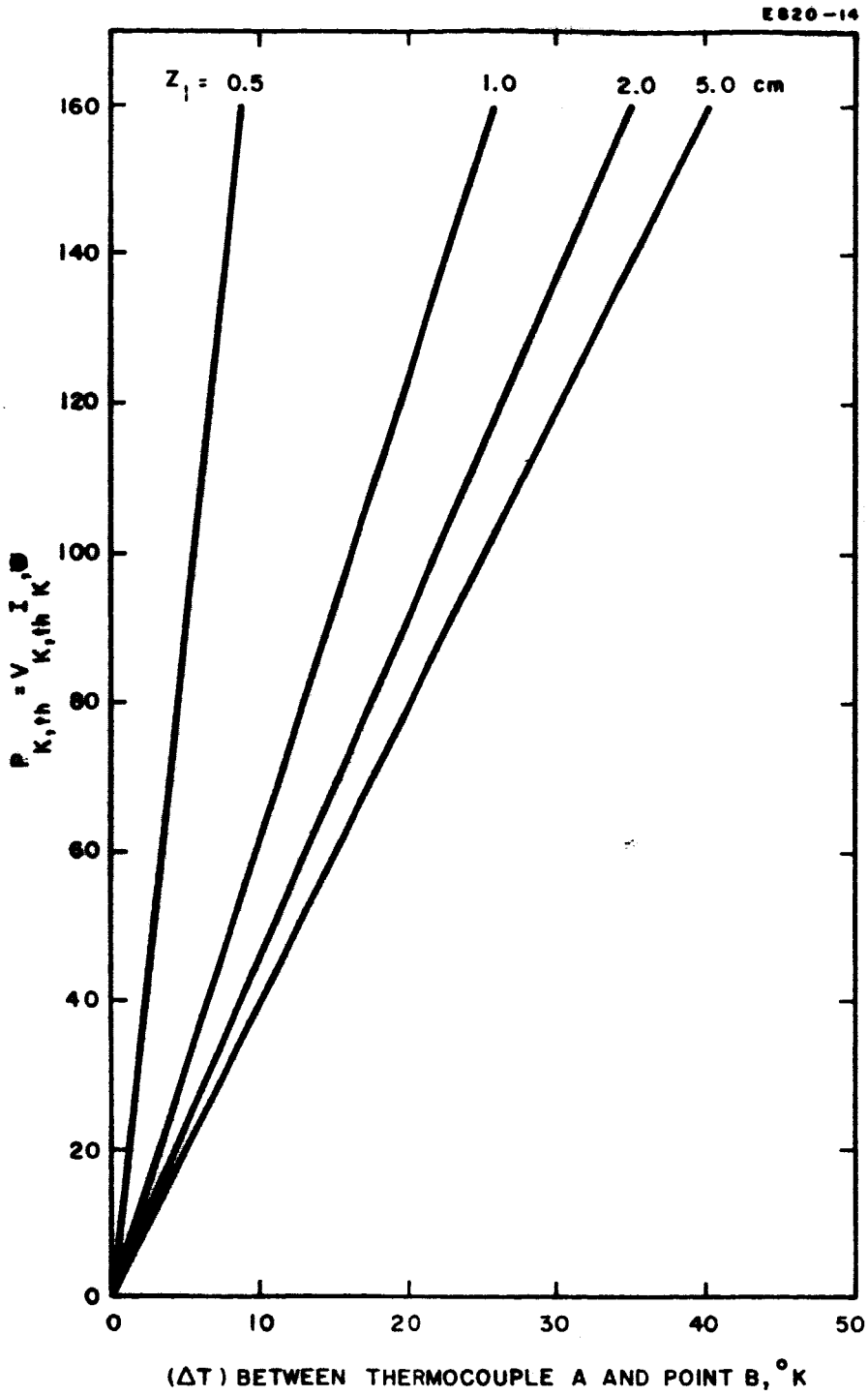

Fig. 16. Temperature difference ΔT between thermocouple point A and point B on cathode as a function of cathode heat flux $V_{K,th} I_K$.

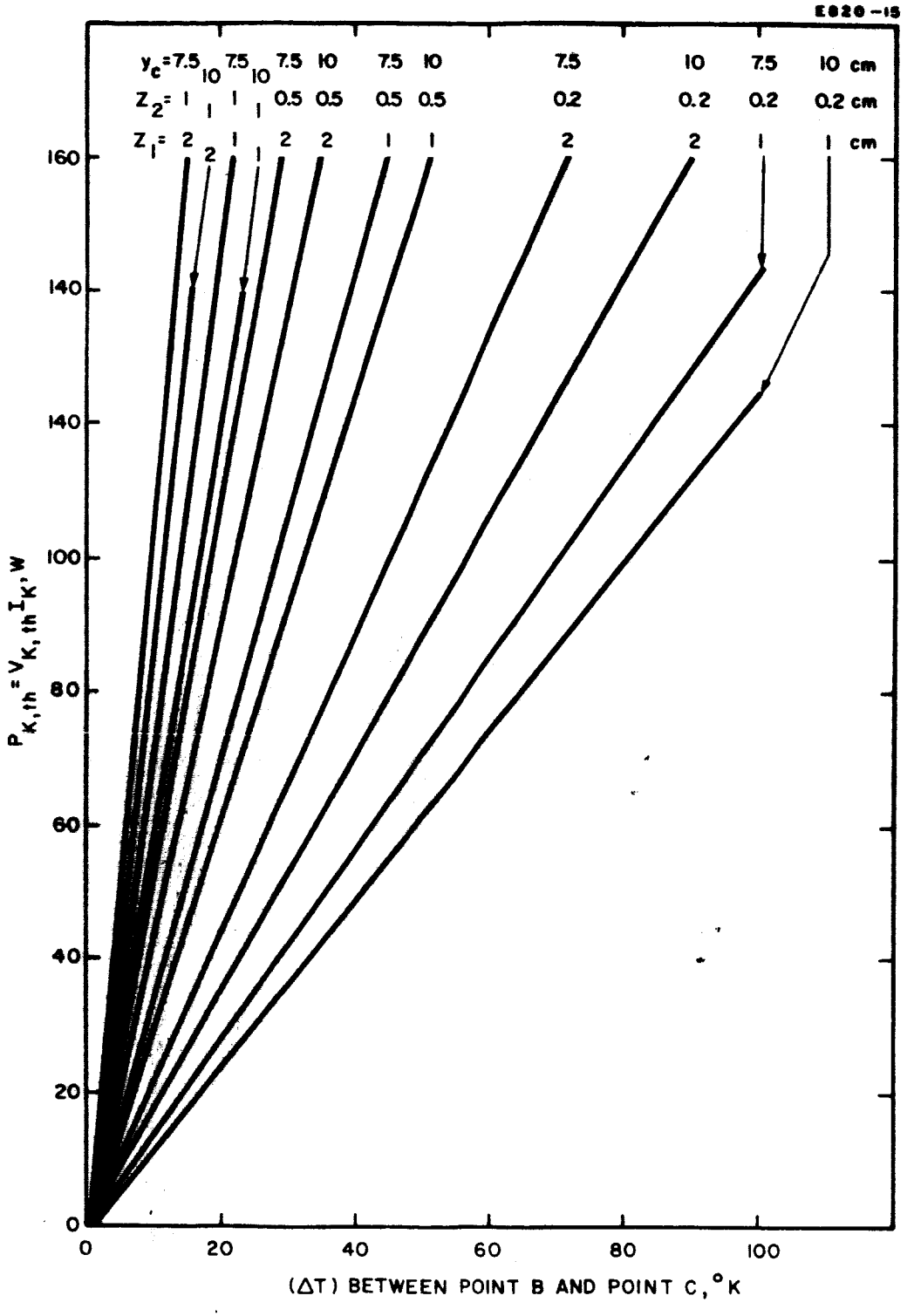

Fig. 17. Temperature difference ΔT between B and C as a function of cathode heat flux $V_{K,th} I_K$.

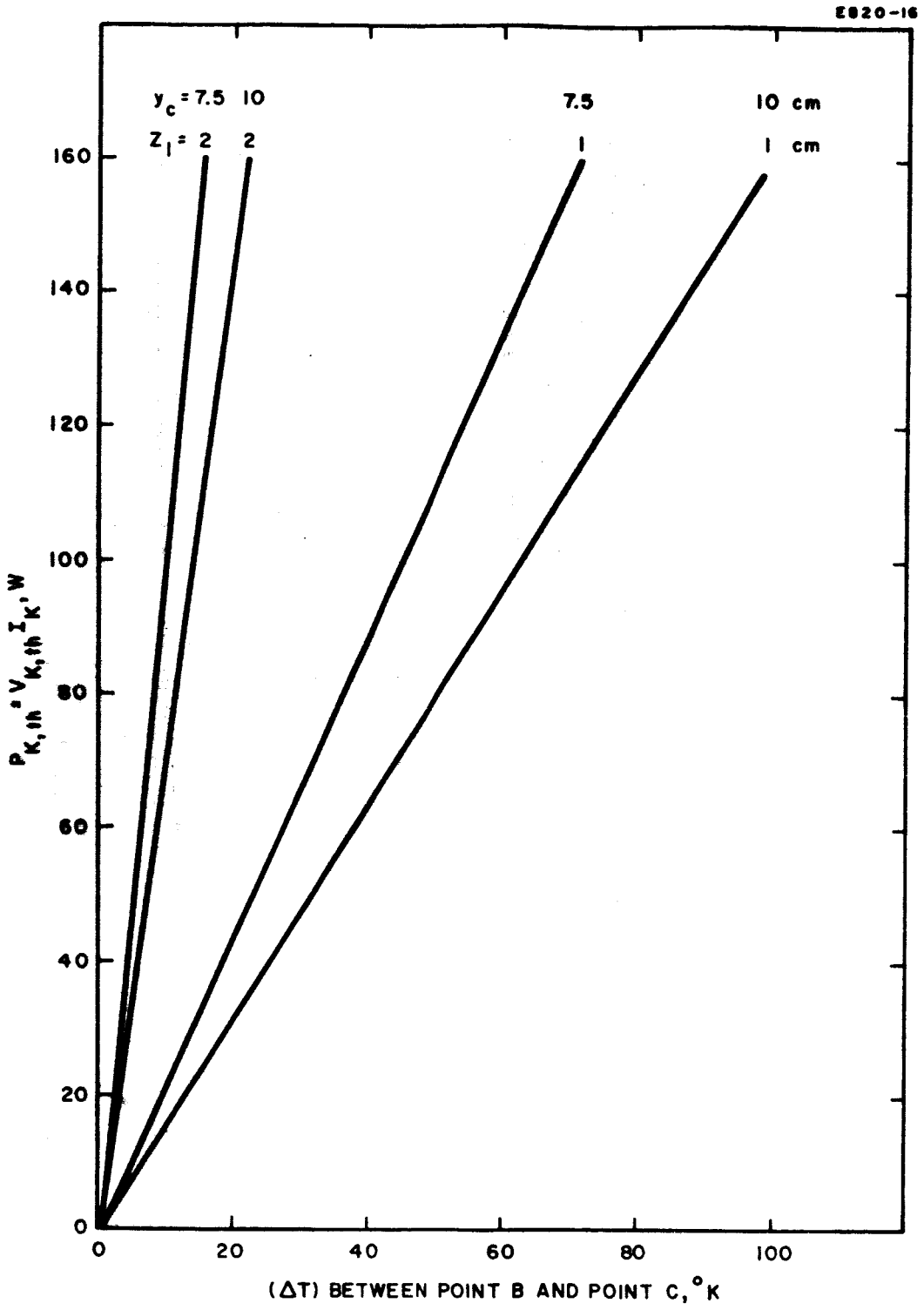

Fig. 18. Temperature difference ΔT between B and C as a function of cathode heat flux $V_{K,th} I_K$.

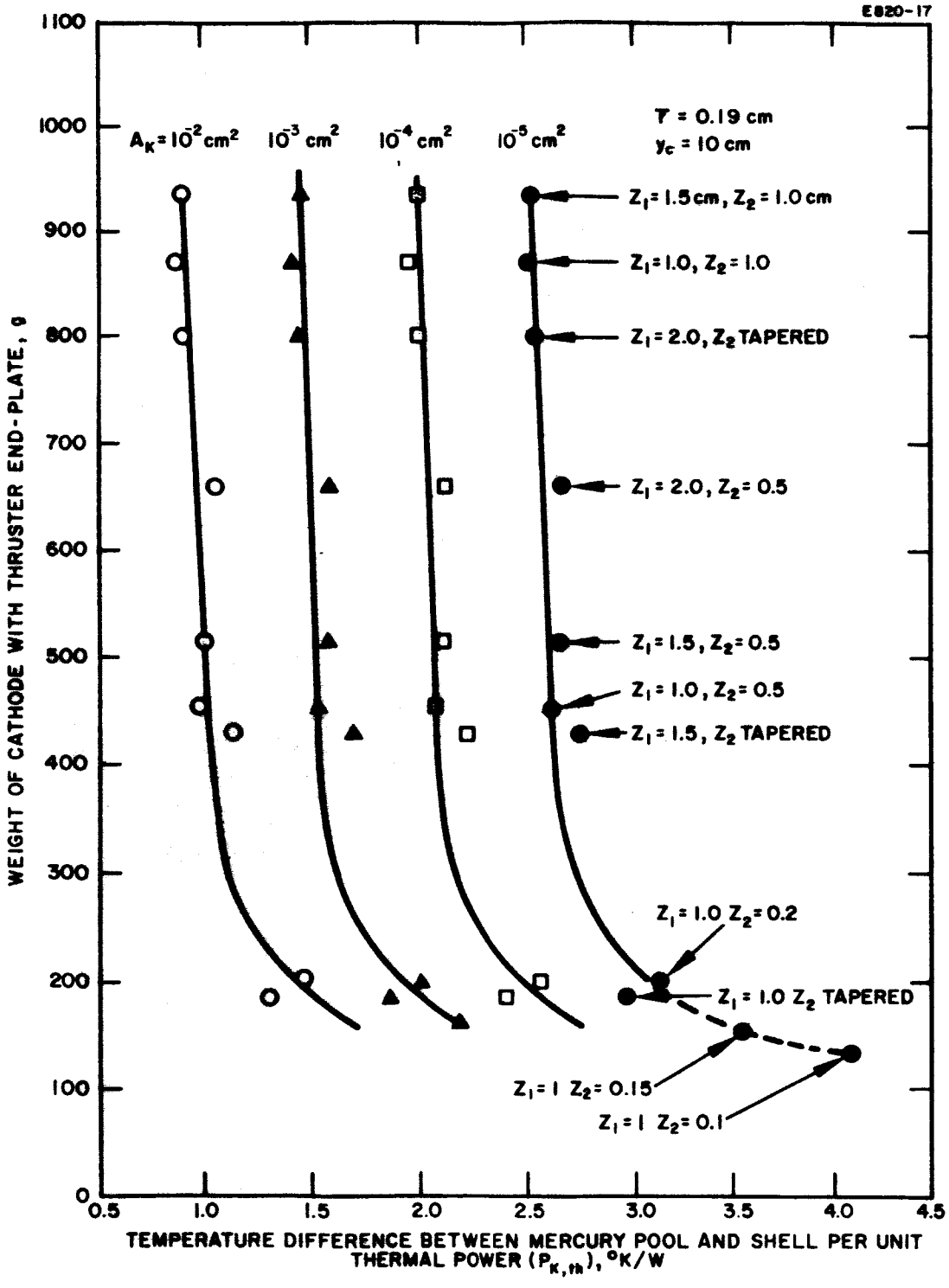

Fig. 19. Temperature difference ΔT between cathode and sink as a function of cathode weight.

F. The Over-All Thruster

In a 20-cm diameter thruster I_B is typically 600 mA; let us assume a mass utilization of 90% at 450 eV/ion. For an electron-to-atom ratio of 12, I_K = 8 A, V_D = 33 V, the total power input to the thruster = 264 W. With a cathode operating at T_{Hg} = 300°C, A_K is equal to 1.6×10^{-4} cm^2.

The temperature of the thruster shell can be expressed as a function of the weight of the cathode plus the shell, assuming a value for the cathode heat input $V_{K,th} \cdot I_K$ and a fixed mercury temperature of T_{Hg} = 300°C. This is shown in Fig. 20 for the typical operating conditions of a 20-cm diameter thruster which are listed above. The three different values of $V_{K,th}$ considered are typical of the values encountered experimentally. With a mercury temperature T_{Hg} of 300°C we see that for any assumed value of $V_{K,th}$ there is a maximum thruster temperature allowed by the cathode structure alone because of its own internal resistance to heat flow. This maximum thruster temperature can be obtained only by use of an infinitely conductive (and therefore infinitely massive) thruster endplate. For an endplate of finite conductance there is necessarily a temperature drop required to drive the heat from the cathode structure to the thruster shell. The curves marked "cathode + shell + heat shielding," which represent the weight of the sum of these components, exhibit an initial decrease in weight as the temperature drop is allowed to increase. This corresponds to a decreasing weight of the cathode backplate.

As the temperature of the thruster shell continues to decrease, the capability of the shell to radiate heat is reduced to a point where it can no longer radiate all of the heat received from the cathode and at the same time accommodate the heat transmitted to it from the anode. This condition can be alleviated by providing heat shielding between the anode and the thruster shell, which constrains the anode heat to radiate forward in the direction of the beam. This shielding permits operation at lower thruster shell temperatures, but not without the penalty imposed by the weight of the heat shielding. We see, therefore, in Fig. 20 that for each value of $V_{K,th}$ there is a particular thruster shell temperature which corresponds to the minimum weight and represents an optimum tradeoff between backplate conductance and heat shielding. We see, for example, that the shell temperature can be as high as 175°C for close to minimum weight, even with $V_{K,th}$ = 7.5 WA^{-1}. For 90% effective shielding between the anode and the aluminum shell, the heat rejected by the shell (including that from the anode) must be about 60 W when $V_{K,th}$ = 5 WA^{-1} and 80 W when $V_{K,th}$ = 7.5 WA^{-1}: this can be achieved easily for an oxidized aluminum shell radiating over 2π steradians into free space.

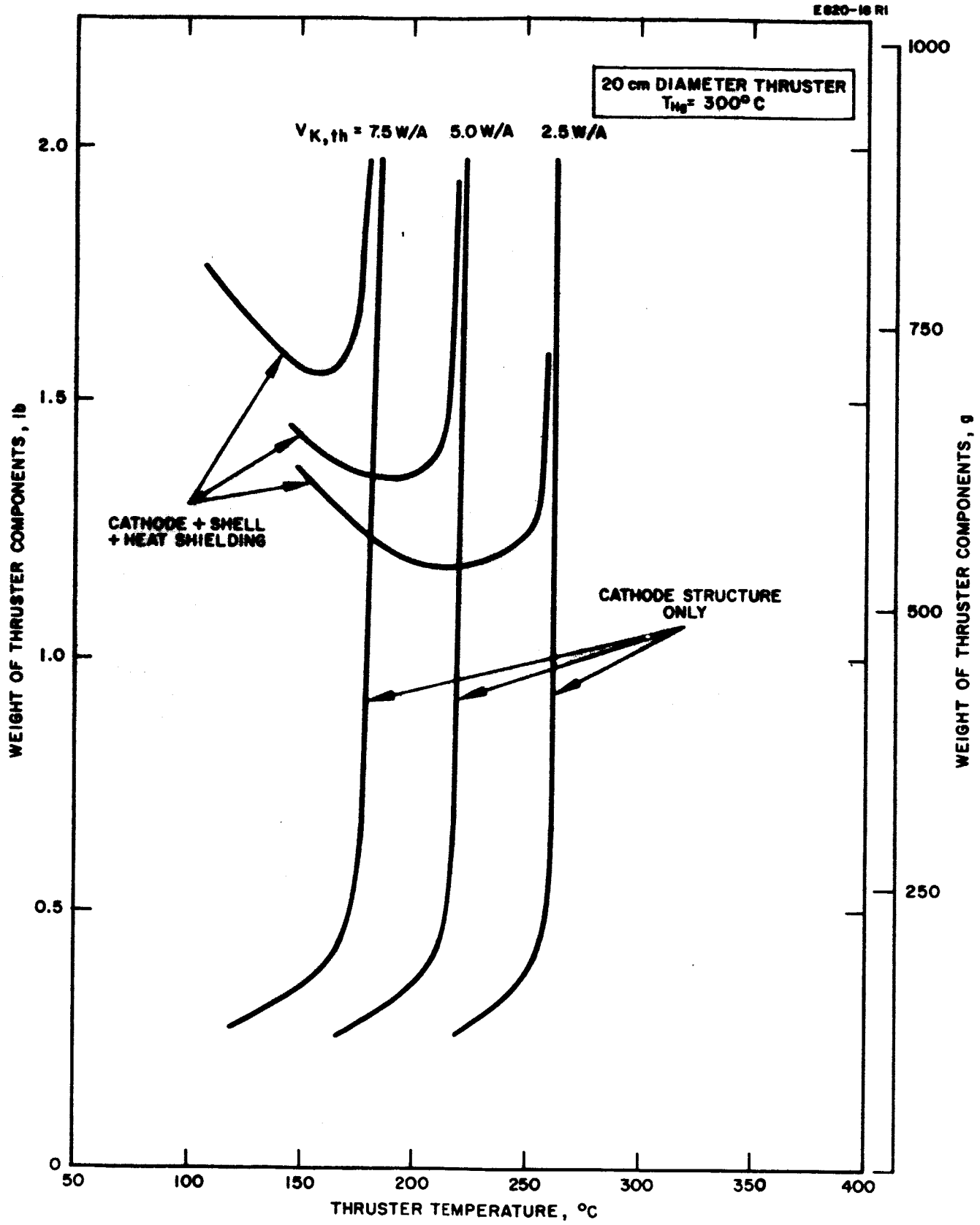

Fig. 20. Thruster shell temperature as a function of weight of thruster components. (η_m = 90%, K_e/K_a = 12, I_B = 600 mA.)

For increased thrust the possibilities exist of either increasing the engine diameter or of mounting engines of, for example, 20 cm diameter, in an array. In the case of a peripheral array of 20 cm thrusters shown in Fig. 21, loss of heat from the thruster shell is equivalent to radiation from about 1/3 of the surface area into a 2π solid angle. Calculations show that the shell can reject the same thermal power as above at temperatures of $\leq 200^{\circ}C$ if the emissivity of the thruster shell is increased to 0.9 by painting with one of several commercially available materials. At this shell temperature the additional rise due to solar exposure at 1 A.U. is $17^{\circ}C$, representing only a 3% perturbation of the absolute cathode temperature T_{Hg}.

G. Conclusions

It can be seen from this analysis that an annular liquid mercury cathode operating at $T_{Hg} = 300^{\circ}C$ can reject heat to a sink at $200^{\circ}C$ at an economical over-all weight. In contrast, the circular cathode experiences a severe temperature drop in the immediate cathode matrix and must be operated with a substantially lower sink temperature; thus it would not be suitable for incorporation into an array, where the radiating portion of the shell area is effectively less than in the freely radiating case.

For a given T_{Hg}, the temperature difference between the cathode and sink depends on the mercury surface area A_K and the annular diameter. These values are determined by the thruster parameters I_B, η_m, and K_e/K_a. Applying the weight optimization procedure outlined above to a 20 cm LM thruster leads to an over-all thruster weight of about 8 lb. This applies to a thruster with 600 mA beam current and $K_e/K_a = 12$. At a specific impulse of 4000 sec, $\eta_m = 90\%$, and a thruster power efficiency of 82% (450 eV/ion), the corresponding weight-to-power ratio would be 5.3 lb/kW. This thruster mounted in a peripheral array would be capable of rejecting the estimated cathode and anode heat flux, even under maximum solar exposure.

E820-1

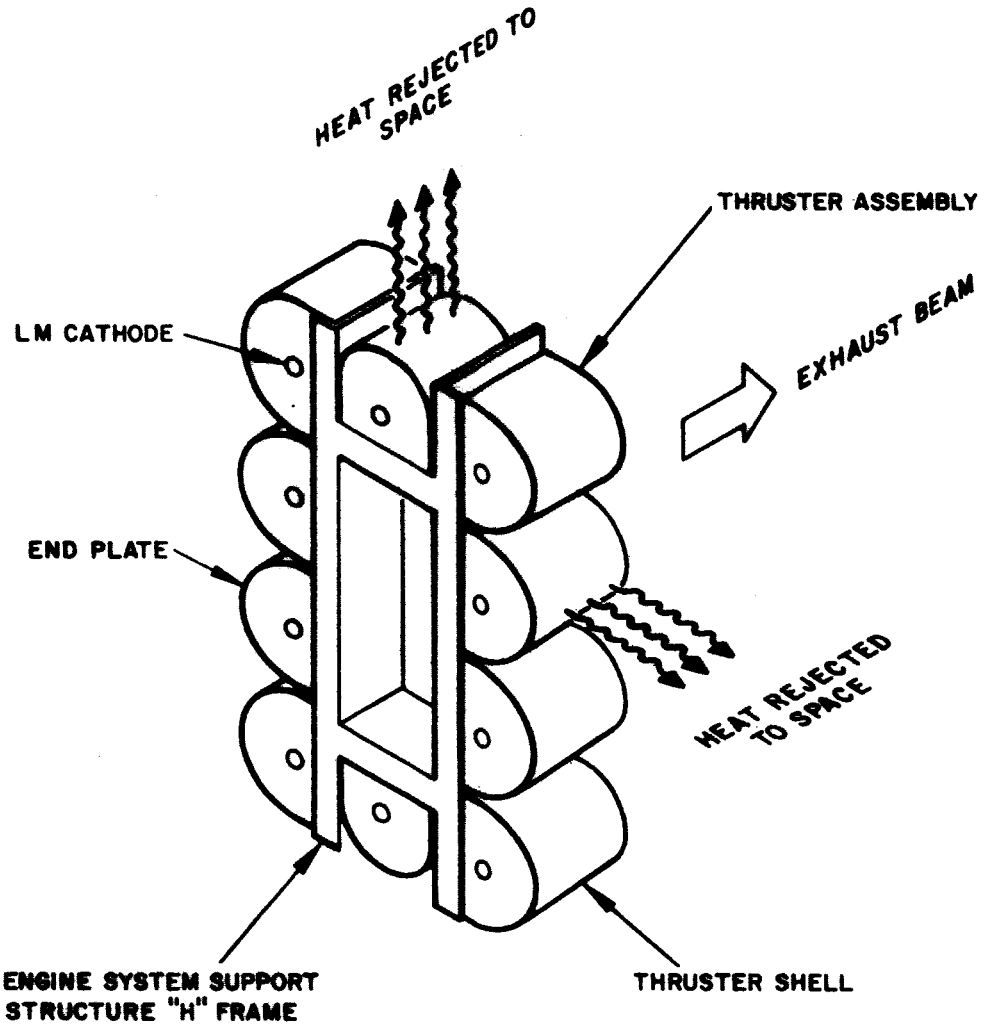

Fig. 21. Peripheral array of 20-cm diameter thrusters.

III. HIGH-TEMPERATURE LM CATHODE RESEARCH AND DEVELOPMENT

A. Main Thruster Cathode

1. Experimental High-Temperature LM Cathode Design

Based on the favorable theoretical results derived in the preceding section for an annular LM cathode, a design implementing this principle was evolved. The success of an annular cathode design depends critically on the uniformity with which it can produce an extremely narrow annular gap. It was felt that the highest degree of uniformity, simultaneously with the least gap width, could be achieved if the two walls of the annular gap were produced separately and then put in the proper relative position by a self-centering geometry of the two components.

The resulting basic design is illustrated by Fig. 22: two cones are first lapped together to a perfect match, and then a surface layer of 2 ... 12 μm (≈ 0.1 ... 0.5 mil) thickness is removed from an annular zone near the tip of the positive cone. This zone is terminated by an annular liquid-metal feed groove. The tip of the positive cone and the face of the part containing the negative cone are shaped so that a certain volume of liquid metal emerging from the narrow annular gap can be contained — a necessity for proper start-up of the cathode at low temperatures. These details are shown in Fig. 3. The remainder of the design, as shown in Fig. 22, is self-explanatory. The material used for the two conical parts is molybdenum, which was chosen because it exhibits the best combination of thermal, mechanical, and chemical properties for this application.

In order to be able to control the temperature of this experimental cathode independently of the temperature of the thruster in which it is used, the cone assembly shown in Fig. 22 is surrounded by a copper heat-exchanger clamp which is fitted to make contact over the entire cylindrical surface of the cone assembly. Copper tubing, serving as a nitrogen gas duct, is brazed to this clamp. Figure 23 is an exploded-view photograph of the cone assembly and the heat-exchanger clamp; this photograph shows the same cathode design as Fig. 22, except for a modified face.

Two annular cathodes were manufactured during the contract period and designated as cathodes No. 25 and 26; their mean annular radii are 0.635 mm and 1.91 mm, respectively. Details of the flow passage geometry of both cathodes were modified in several steps, and the following notation is used in Section III-A-5 to distinguish the

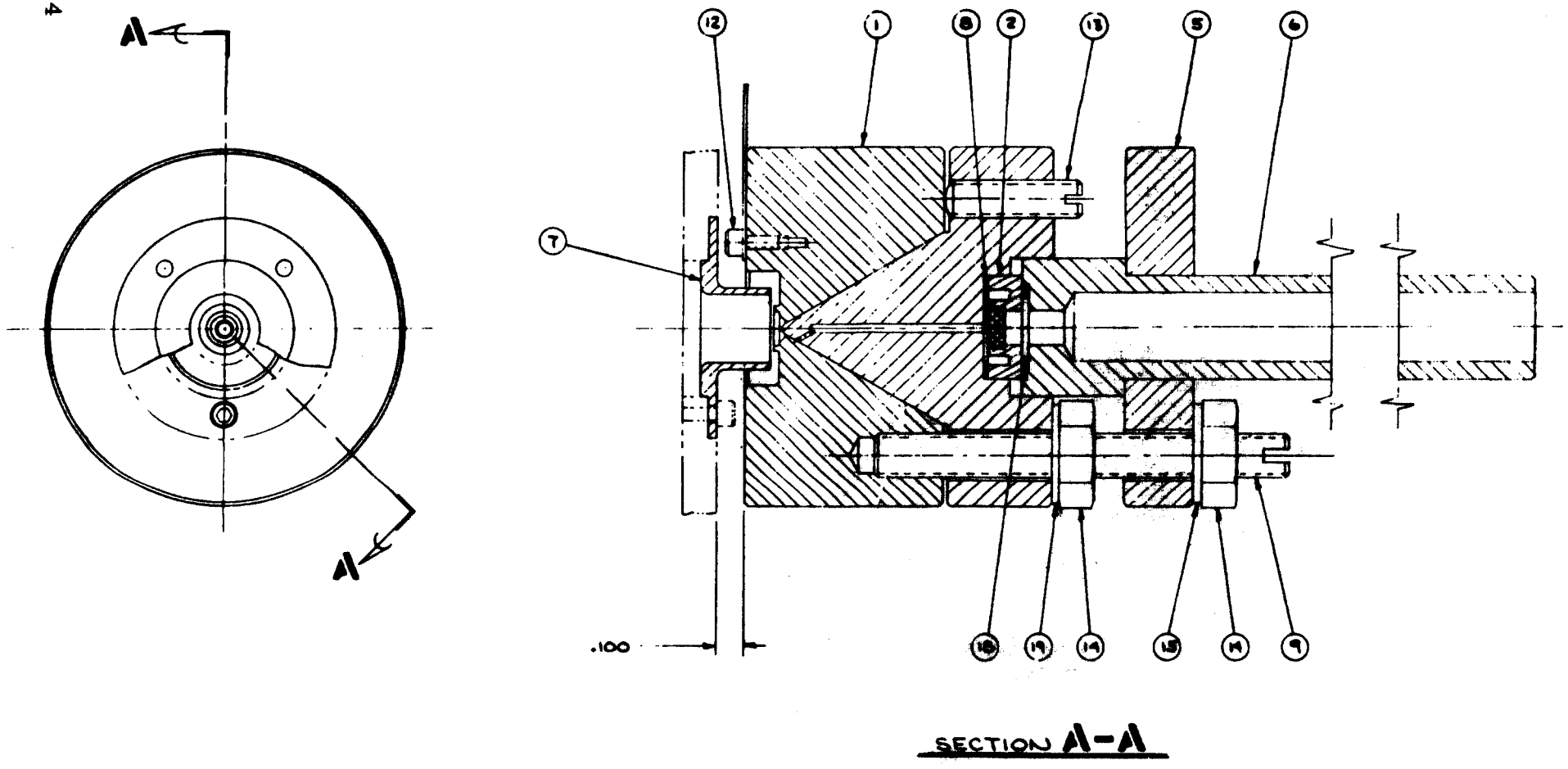

Fig. 22. Annular LM Cathode Design.

Legend: 1. Cone assembly, 2. Flow impedance, 5. Feed tube flange, 6. Feed tube, 7. Non-magnetic insert (in magnetic thruster end plate), 8. Metal gasket, 9. Stud, 12. Thermocouple screw, 13. Set screw (for cone disassembly), 14. Nut, 15. and 19. Spring washers, 18. Metal O-ring.

M5128

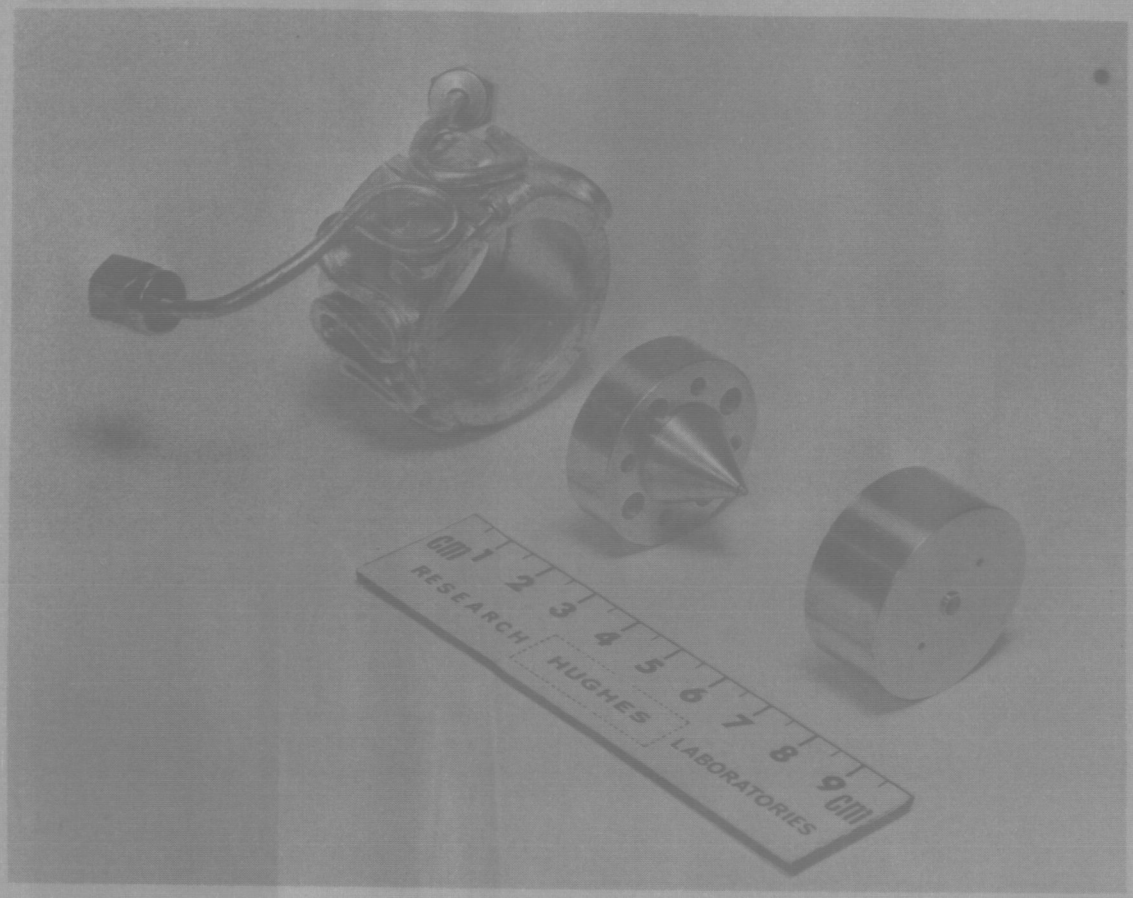

Fig. 23. High-temperature annular LM cathode cones and heat-exchanger clamp.

various stages of modification: "I" indicates the original shape as shown schematically in Fig. 3. "II" designates modification of the uniformly narrow mercury flow passage shown in Fig. 3 to a narrow passage of minimum depth, fed by a wider passage. "III" indicates stage-II modification plus truncation of the inner cone of the pool-keeping structure at the downstream end of the narrow flow passage. "IV" indicates widening of the entire flow passage (see Section III-A-4).

2. Electrical Pulse Igniter

The introduction of high voltage pulses for arc initiation contributed to the successful evaluation of LM cathodes at high temperature. With the new ignition circuit, cessation of the arc current energizes a relay which in turn completes a circuit furnishing rapid, high voltage pulses to a stationary igniter electrode placed in front of the cathode. The arc usually needs only one pulse to restart under normal operation, and placement of the igniter electrode relative to the cathode does not demand more than reasonable initial adjustment.

The electrical pulse ignition system is fully applicable to thruster operation. A flight-type system will use a vacuum potted pulse transformer (also demonstrated) and silicon controlled rectifiers instead of electro-mechanical relays.

3. Derivation of a Normalized Performance Parameter

In order to make meaningful comparisons of cathode performance between different cathodes or before and after modifications of cathode geometry, allowance must be made for different operating conditions. This can be done by specifying a fixed set of normalized operating conditions, choosing one suitable performance parameter, and transforming its measured value to a normalized value. We have selected the temperature of the radiating thruster shell, the thermal resistance of the thruster end plate, and the current drawn from the cathode as the fixed conditions, because these parameters are dictated by thermal and weight considerations regarding the spacecraft and by thruster (rather than cathode) design. We have chosen the electron-to-atom emission ratio as the performance factor to be normalized (while retaining the measured value of the specific thermal loading of the cathode), because on the one hand this ratio is affected by changes in all other parameters, thus representing a compound measure of cathode performance, and on the other hand its normalization is amenable to analytical formulation without undue approximations.

We use the following notation:

K_e/K_a ≡ electron-to-atom emission ratio

I_K ≡ current drawn from cathode

$P_{K,\,th}$ ≡ thermal power delivered to cathode

$V_{K,\,th} = P_{K,\,th}/I_K$ ≡ equivalent voltage, expressing specific thermal loading of cathode

p_{Hg} ≡ vapor pressure over exposed mercury surface in cathode

T_{Hg} ≡ temperature of exposed mercury surface in cathode

T_K ≡ temperature of cathode at thermocouple location

T_T ≡ temperature of radiating thruster shell

$\Delta_K T = T_{Hg} - T_K$ ≡ temperature difference within cathode

$\Delta_T T = T_K - T_T$ ≡ temperature difference within thruster end plate

$R_{th,\,K} = \Delta_K T/P_{K,\,th}$ ≡ thermal resistance of cathode

$R_{th,\,T} = \Delta_T T/P_{K,\,th}$ ≡ thermal resistance of thruster end plate

e ≡ elementary charge

Subscripts:

m ≡ measured

n ≡ normalized

First, we note that

$$K_e = I_K/e \quad \text{and} \quad K_a \propto p_{Hg}(T_{Hg}) \ ,$$

where the latter is true for a fixed position of the exposed mercury surface in the pool-keeping structure. Next, we observe that we have the following functional dependences:

$$T_{Hg} = T_{Hg}(T_K, I_K, V_{K,\,th}, R_{th,\,K}),$$

and

$$T_{Hg} = T_{Hg}(T_T, I_K, V_{K,\,th}, R_{th,\,K}, R_{th,\,T}) .$$

Therefore, we can write for the measured and normalized electron-to-atom emission ratios, respectively,

$$\left(\frac{K_e}{K_a}\right)_m \propto \frac{I_{K,\,m}}{p_{Hg}[T_{Hg}(T_{K,\,m}, I_{K,\,m}, V_{K,\,th,\,m}, R_{th,\,K})]}$$

$$\left(\frac{K_e}{K_a}\right)_n \propto \frac{I_{K,\,n}}{p_{Hg}[T_{Hg}(T_{T,\,n}, I_{K,\,n}, V_{K,\,th,\,m}, R_{th,\,K}, R_{th,\,T})]} .$$

In writing these expressions, we make the assumption that a fixed position of the exposed mercury surface results in a fixed value of the specific thermal loading. At least for the current range to which the normalizing procedure will be applied, this appears to be a reasonable approximation. We then have the following self-explanatory equations:

$$\left(\frac{K_e}{K_a}\right)_n = \left(\frac{K_e}{K_a}\right)_m \cdot \frac{I_{K,\,n}}{I_{K,\,m}} \cdot \frac{p_{Hg}[T_{Hg}(T_{K,\,m} I_{K,\,m}, V_{K,\,th,\,m} R_{th,\,K})]}{p_{Hg}[TH_g(T_{T,\,n}, I_{K,\,n}, V_{K,\,th,\,m}, R_{th,K} R_{th,\,T})]}$$

$$T_{Hg} = T_T + \Delta_T T + \Delta_K T = T_K + \Delta_K T$$

$$\Delta_T T = I_K V_{K,\,th} R_{th,\,T}$$

$$\Delta_K T = I_K V_{K,\,th} R_{th,\,K} .$$

With these, plus a table or graph for the saturated vapor pressure of mercury as a function of temperature, we can now present our experimental results in a normalized form; we have done this in Section III-A-5.

From the standpoint of purely thermal requirements in the thruster applications, a cathode performs better as its $(K_e/K_a)_n$ increases; from the standpoint of both thermal and efficiency requirements, cathode performance must be judged in terms of both a high $(K_e/K_a)_n$ and a low $V_{K,th}$.

4. Vapor Feeding of High-Temperature LM Cathodes

Experiments performed some time ago under Company-sponsored programs have shown that circular LM cathodes operating at high currents ($\approx$ 150 A) and high degrees of spot-pattern contraction (corresponding to current densities $\gtrsim 10^4$ A cm^{-2} averaged over the exposed mercury area) can switch under certain thermal conditions spontaneously into a different mode, which will be referred to here as the "diffuse spot-pattern" or "DSP" mode in order to distinguish it from the normal "linear spot pattern" or "LSP" mode. In these experiments a high current discharge was started with the mercury surface being large compared with the feed channel area. As the mercury contained in the pool-keeping structure was used up, the cathode spot pattern shrank to the size of the channel, and then the arc spot pattern became diffuse (i.e., the cathode glow was distributed quite uniformly over an area, rather than concentrated along a line). In this mode the mercury surface is below the mouth of the channel, but copious evaporation keeps the discharge supplied with vapor.

We believe that in this mode the random motion of the individual arc spots is distributed over the entire luminous area, rather than restricted to a line, so that the time-averaged current density in the diffuse spot pattern is reduced by orders of magnitude from the level associated with the linear spot pattern.

The spots are believed to exist by virtue of a transient condensation of mercury vapor on the walls of the pool-keeping structure. It may not be necessary for a heavy condensation of mercury vapor to occur because electron emission (if it is caused, for example, by excited mercury atoms impinging on the cathode) could occur without a complete, macroscopic covering of mercury over molybdenum. The

work function of molybdenum (4.4 eV) is less than the metastable potential of mercury (4.67 eV), so that electron emission is energetically possible at a reasonable yield.*

On the basis of these considerations, we concluded that it should be possible to separate spatially the region where vapor is evolved from a free mercury surface and the region where transient recondensation of this vapor permits electron emission in the diffuse spot-pattern mode — in other words, it should be possible to vapor-feed (rather than liquid-feed) an LM cathode operating in the DSP mode.

This possibility is of special interest because it promises several advantages over liquid-fed LSP-mode LM cathodes in thruster operation:

(a) Higher thruster efficiency and lower specific thermal loading should result from thermally decoupling the pool-keeping structure from the evaporator, because the required electron-to-atom emission ratio may be obtained with less vapor flow constriction (and hence, less plasma losses) downstream from the electron-emitting zone.

(b) A vapor-fed LM cathode could use the same feed system and isolator as is used for electron-bombardment thrusters with other cathode types, thus permitting more flexibility in cathode choice for these thrusters up to late stages of design freezing.

(c) It may be possible to achieve such high electron-to-atom emission ratios that only a fraction of the total expellant flow needs to be fed through the cathode. (This is a consequence of the reduced thermal power input density in the DSP mode, compared with the LSP mode.) The resulting design freedom for the expellant injection pattern should result in additional thruster efficiency improvements, as well as in complete interchangeability between LM and other cathodes, without any thruster modifications.

---

*Optically similar phenomena, observed on spot anchors with conventional pool cathodes at much lower currents and in the presence of strong axial magnetic fields, were described by C.G. Smith[6] and K.G. Hernqvist[7]; the latter author termed this type of discharge the "dispersed" or "D" mode and established an upper current density limit of $\approx 10^2$ A cm^{-2} for this mode. Our much higher current densities, as well as other observations reported below, lead to the conclusion that the dispersed mode and the diffuse spot-pattern mode are not identical. One might say that in the D mode the spot itself is dispersed over a relatively large area, resulting in a considerable change in the emission mechanism, while in the DSP mode only the pattern of the random spot motion is diffuse, leaving the conditions during the life of an individual spot substantially unchanged from those prevailing in the LSP mode.

The listed advantages have prompted us to substitute a vapor feed system for the liquid feed system used with Cathode No. 26 in order to obtain some first-order experimental results. The feed system conversion was accomplished by omitting the flow impedance, electron-beam welding a stainless-steel vaporizer mesh into the feed line, and wrapping a heater around the feed line portion between vaporizer and cathode. The same mercury reservoir was used as with the liquid feed system, thus permitting accurate flow rate measurements within time intervals of a few minutes. The feed system was kept under a constant pressure ($\approx$ 1 psig), and the flow rate was adjusted by varying the vaporizer temperature. Even though no modifications on the cathode proper were made, the results of our experiments are extremely encouraging; they are listed in the following section. The electrical pulse ignitor proved to be usable also for the vapor-fed LM cathode without modification. One important observation is that the discharge starved out when the temperature was raised too high for a given flow rate, indicating the importance of transient condensation as postulated above for the DSP mode, and in contrast to the expectations for Hernqvist's D mode.

Following these successful experiments Cathode No. 25 has been modified for operation in the DSP mode with vapor feeding. The conversion included a modification of the pool-keeping structure aimed at lowering the specific thermal loading of the cathode; the width of the conical-shell shaped mercury (vapor) feed channel was increased by a factor of approximately three in order to reduce the wall losses from the constricted plasma which couples the cathode spot(s) to the main discharge plasma. (Note that this widening is not permissible for a liquid-fed cathode.) The experimental results obtained with this cathode (and listed below) have fully confirmed our expectations.

We have also obtained experimental evidence that the high-temperature LM cathode, when operating with the free mercury surface deeply retracted into the feed channel or when vapor-fed, does not emit electrons by the same mechanism as the mercury vapor hollow cathode described by Hernqvist.[8] This was demonstrated by modifying one of our cathodes so that it could actually be operated in the hollow-cathode glow discharge mode, and by observing that the electrical characteristics were totally different from those of the LM cathode in its normal operating modes.

The modification consisted of clamping a thin tungsten sheet with a small opening over the downstream end of the pool-keeping structure of Cathode No. 26 (stage III with vapor feeding). This created a cavity which was filled with mercury vapor when the feed system was turned on. Actuation of the electrical pulse igniter produced a stable discharge of $\approx$ 5 mA at $\approx$ 300 V discharge voltage. (Hernqvist's cathode, with different dimensions, produced $\approx$ 4 mA at 300 V.)

The high discharge voltage persisted even when the anode was placed directly in front of the cavity exit opening, thus indicating that neither thermionic nor liquid-metal spot emission was taking place. Instead, the electrons were liberated from the cavity walls by ion bombardment from the plasma region inside, which was essentially at anode potential. Consequently, the bombarding ions cause considerable sputtering damage, and when the 3-mil tungsten sheet was removed after two days of operation, the exit aperture was found to be enlarged to several times its original size.

This is in sharp contrast to the conditions prevailing when a high-temperature LM cathode is operated in either the linear or the diffuse spot-pattern mode. Here, only up to ≈ 10 V potential difference (less than the sputtering threshold) are available to accelerate the ions which bombard the walls of the pool-keeping structure. Hence the life of high-temperature LM cathodes can be expected to be of the same order of magnitude as the (demonstrated) life of the low-temperature version.

5. Test Results in Diode Operation

A comprehensive presentation is given in Table I of all those high-temperature LM cathode diode measurements which included determinations of the specific thermal loading. The table lists the directly measured parameters and the normalized electron-to-atom emission ratio as defined in the preceding section. For the smaller of the two cathodes the normalization has been carried out for two cases: (a) Operation in a 15-cm diameter thruster at $I_{K,n} = 6$ A, with $T_{T,n} = 225^{\circ}C$ and $R_{th,T} = 0.7^{\circ}K\ W^{-1}$. (b) Operation in a 20-cm diameter thruster at $I_{K,n} = 8$ A, with $T_{T,n} = 250^{\circ}C$ and $R_{th,T} = 1.0^{\circ}K\ W^{-1}$. Both cases correspond to thrusters operating in relatively dense clusters (see Section II), and case (a) represents a relatively unfavorable discharge-to-beam current requirement. For both cases and both cathodes, $R_{th,K} = 1.66^{\circ}K\ W^{-1}$ was assumed (see Section II).

Inspection of Table I leads to the following conclusions:

1. Cathode No. 25-II can meet and exceed all temperature and K_e/K_a requirements of 15-cm thrusters, even under unfavorable conditions.

2. With this cathode, further minimization of $V_{K,th}$ (and the associated discharge voltage differential) can be expected to result in thruster efficiency improvements on the order of 100 eV/ion for case (a).

3. The same cathode cannot meet equally rigorous requirements for operation in a 20-cm thruster.

TABLE I

Diode Test Results
(All tests have lasted for several hours (typically 4 to 7))

Test No.	Cathode Type	Feed Method	$T_{K,m'}$ °C	$I_{K,m'}$ A	$V_{K,th,m'}$ WA^{-1}	$\left(\frac{K_e}{K_a}\right)_m$	$\left(\frac{K_e}{K_a}\right)_n$ 15-cm	$\left(\frac{K_e}{K_a}\right)_n$ 20-cm
1	25-II	Liquid	250	5.0	4.7	10	11	4.7
2	"	"	300	5.3	11	12	18	5.7
3	"	"	"	8.6	12	10	25	6
4	"	"	"	9.0	10	10	28	7.6
5	26-I	"	"	12.8	7.6	13		17
6	"	"	"	9.8	6.1	16		18
7	"	"	"	9.2[a]	10.6	17		12
8	26-III	"	"	15.8	8.3	21		34
9	"	"	"	10.5	7.1	41		45
10	"	"	"	21	9.7	31		83
11	"	"	"	23	9.7	28		91
12	"	"	375	16.3	8.7	20		70
13	26-III	Vapor	310	14.0	6.6	10	n.a.[b]	n.a.[b]
14	"	"	300	11.3	5.9	10	"	"
15	25-IV	"	"	6.4	6.3	11	"	"

[a] Spot pattern only half circle.

[b] The normalization principle (Section III-A-3) is limited to the liquid-fed case.

4. Cathode No. 26 can meet and, in its stage III considerably exceed, all thermal and emission ratio requirements of 20-cm thrusters, including the most unfavorable conditions. It should perform satisfactorily also in considerably larger thrusters.

5. In liquid-fed operation of this cathode, minimization of $V_{K,th}$ can be expected to result in thruster efficiency improvements on the order of 50 eV/ion for case (b). This conclusion is in excellent agreement with the experimental comparison of Cathode No. 26 with the water-cooled life-test cathode (see Section IV-B-1).

6. Approximately one-half of this possible improvement may already be realizable by vapor-feeding of the same cathode, as evidenced by tests No. 13 through 15. The latter represents an improvement by a factor of ≈ 1.8 over the performance of the same cathode in liquid-fed operation. (No thruster tests have been performed yet.)

7. The monotonic increase of the normalized performance parameter as a function of cathode geometry evolution fully justifies the steps taken during this evolution.

8. The table clearly shows the trade-offs between the various parameters. For example, test No. 7, compared with No. 6, shows the detrimental effect on $(K_e/K_a)_n$ and $V_{K,th,m}$ caused by partial utilization of the available spot-pattern length; and test No. 12 shows the feasibility of operation at even-higher temperatures.

B. LM Cathode Neutralizer

1. Introduction

The operating temperature of an LM cathode neutralizer in space is expected to be in the vicinity of 100°C, assuming that it can radiate waste heat only from its exposed face. It was one objective of this effort to demonstrate that LM cathode neutralizers can operate at such temperatures with high electron-to-atom emission ratios and high electrical efficiency.

We have previously operated an LM cathode neutralizer at room temperature for over 500 hours as part of a thruster life test.*

*Under Contract NAS 3-6262.

This neutralizer is shown in partial cross section in Fig. 24. During the 500-hour test a constant mercury flow was maintained by the same method as with the main thruster cathode, i.e., a constant pressure was applied to the storage reservoir, and a porous-tungsten flow impedance upstream of the pool-keeping structure permitted a mercury flow to pass which was (within the flow range of interest) a smooth function of the applied pressure. In order to shift the flow range where this smooth flow-pressure dependence exists to the level required for a neutralizer (one to two orders of magnitude below that of the main thruster cathode), it was necessary to use a flow impedance of ≈ 40 times higher value than that of the main thruster cathode. This higher impedance level was achieved with porous tungsten of the standard porosity by increasing the thickness of the flow-impeding layer by a factor of 20, and by reducing its cross-sectional area by a factor of 4.

For the test mentioned above, the neutralizer was equipped with a mechanical automatic igniter, consisting of a solenoid-actuated tungsten tip which dipped into the exposed liquid mercury when the arc current was interrupted; it was subsequently pulled out in order to restrike the discharge. While this type of igniter performed to full satisfaction on the main thruster cathode during the life test, its use on the neutralizer left much to be desired. Because of the approximately equal diameters of igniter and neutralizer pool-keeping structure, this mechanical action caused splashing of a considerable fraction of the small amount of liquid mercury contained in the pool-keeping structure when operating at the high K_e/K_a and low current wanted for neutralizer service. This, in turn, had two detrimental effects: (a) It permitted the arc to run on the splashing mercury globules outside the pool-keeping structure, resulting in frequent arc extinctions (followed by more splashing by the igniter and thus perpetuating the situation). (b) It limited the obtainable effective electron-to-atom emission ratio to a level far below the design value (even though the latter had been confirmed in experiments using careful manual ignition).

During this contract period the electrical pulse igniter circuit described in Section III-A-2 was adapted to operation with the neutralizer cathode, the only major difference being in the sensitivity and current carrying capability of the discharge current sensor. The use of a pulse igniter immediately resulted in stable neutralizer operation without the frequent arc extinctions experienced before.

It has been found that our LM cathode neutralizer can be operated in two different feed modes, depending on the cut-off characteristics of the flow impedance used. If the range of the smooth flow-pressure dependence extends down to the flow rates desired, continuous feeding from the pressurized storage reservoir can be employed.

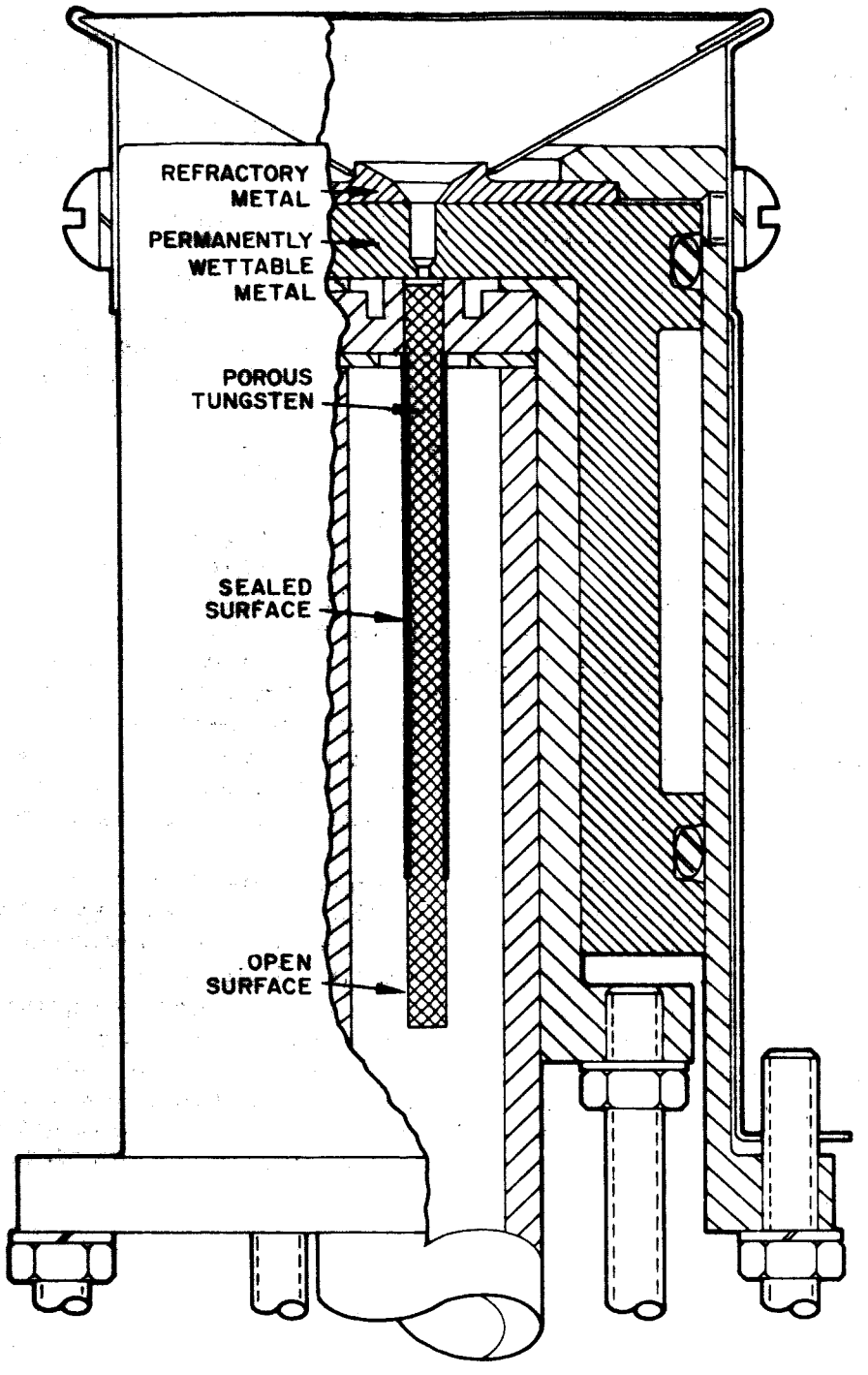

Fig. 24. Schematic cross-section of LM cathode neutralizer, not to scale.

(Results obtained with this technique are described in Section III-B-3.) On the other hand, if the flow rate remains too high all the way down to the cut-off point, feeding can be accomplished as described in the following section. Either method could be used in a flight-type neutralizer system.

2. Operation in the Capillary-Feed Mode

It was observed that when the feed pressure was first raised above the flow threshold and then lowered below the flow threshold of the porous-tungsten flow impedance (while monitoring the presence or absence of flow into the impedance with the position indicator of the reservoir piston*), mercury continued to be supplied to the neutralizer cathode at a uniform rate for several hours after the flow into the impedance had stopped. This was explained as the action of a small "capillary feed system," with the void volume of the porous-tungsten flow impedance serving as the mercury reservoir (see Fig. 24) and the permanently wettable portion of the bimetal pool-keeping structure serving as the wick. The rate of mercury flow into the pool-keeping structure was found to be adjustable by varying the temperature of the heat-exchanger jacket (which controls the temperature of both the pool-keeping structure and the porous tungsten rod). The required temperatures were between 65 and 80°C. Thus, feed rates compatible with discharge currents ranging from 250 mA to several amperes have been produced, and stable operation without discharge extinction has been demonstrated for many hours.

In order to measure the approximate electron-to-atom emission ratio for neutralizer cathode operation in the capillary-feed mode, we have operated the cathode continuously from the time when the capillary reservoir was refilled until the time when the cathode starved out. Assuming on the one hand that starvation meant absolute depletion of all voids in the porous tungsten rod and in the pool-keeping structure, and on the other hand that the absence of piston movement meant that no mercury was entering the porous tungsten rod, we have computed K_e/K_a from the known void volume and the operating time to starvation. The typical diode test results obtained are given in Table II.

*A complete description of this technique of mercury flow measurement is given in the Summary Report, Contract No. NAS 3-4118.

TABLE II

Neutralizer Diode Test Results (Capillary-Feed Mode)

Neutralizer Current, A	Discharge Voltage, V	K_e/K_a	Run Duration, hours
2.5	18.5	87	1.58
1.5	21.5	110	3.33
1.45	21	59	1.85
0.6 and 1.5 (0.9 ave.)	20.5	94	4.75
0.6	20	53	4

The validity of the electron-to-atom ratios listed above was confirmed by the very similar results described in the following section.

3. Operation in the "Normal" Feed Mode

Using a flow impedance with a sufficiently low threshold flow, feed rates appropriate for the neutralizer range have been maintained steadily for several days, and the neutralizer has been operated stably in many diode runs of several hours duration. Excellent electron-to-atom emission ratios were obtained, simultaneously with low discharge voltages, at currents ranging down to 250 mA. In these runs the heat-exchanger temperature was $\approx 82^{\circ}C$ (and the neutralizer face temperature several degrees higher), limited by the use of a water thermostat. The results are summarized in Table III.

TABLE III

Neutralizer Diode Test Results
("Normal" Feed Mode)

Neutralizer Current, A	Discharge Voltage, V	K_e/K_a	Run Duration, hours
1.5	20.5	62	3.5
1.0	21	40	6
1.0	21.5	80	1
0.6	20	114	1
0.5	21	37	9
0.4	20.5	34	2.5
0.3	20.5	57	1
0.25	20	55	3

It should be noted that no feed-back loop existed for controlling the flow rate; instead, these results were obtained simply by adjusting the feed pressure for the proper flow rate at the beginning and keeping the pressure constant during the run.

In conclusion, it can be stated that stable LM cathode operation in the neutralizer current range has been demonstrated, with very attractive electron-to-atom emission ratios and power expenditures, at temperatures close to the equilibrium temperature of a neutralizer which is cooled only by radiation from its face. In addition the discharge voltages (and hence, power expenditures) listed above are very close to those observed in thruster testing of LM cathode neutralizers.[9]

IV. THRUSTER TEST RESULTS

A. Introduction

Very successful demonstrations of high-temperature cathode operation in electron-bombardment thrusters have been achieved during the contract period. Two different thrusters were employed for these experiments: (a) The 20-cm diameter modified LeRC thruster which had successfully undergone a 4,000-hour life test[4, 9] (with an LM cathode operating at $\approx 35^{o}C$) was available as a versatile test bed; it is shown, equipped with a high-temperature LM cathode, in schematic cross section in Fig. 25. (b) A 15-cm diameter thruster, shown in Fig. 26 with permanent magnets, had been equipped with iron-core electromagnets in order to obtain variability of the magnetic field while retaining the field geometry typical for a permanent-magnet unit; this thruster conforms closely with the requirements for a flight-type system and has served to demonstrate the compatibility of our high-temperature cathode design with these requirements. Both thrusters were used in performance-optimization experiments as well as for diagnostic measurements.

B. 20-cm Diameter Thruster Experiments

1. Comparative Measurements with High and Low Temperature Cathodes

Annular Cathode No. 26 was installed in the 20-cm thruster as shown in Fig. 25. The baffle consisted of an annular opaque zone of fixed dimensions, plus a central opaque zone of variable diameter; the axial position of the baffle was also variable. This baffle had also been used during the last 500-hour increment of the life test, where it had led to a reduction by one-third of both the optimum K_e/K_a and the heat load of the cathode, simultaneously with a 23% reduction of the source energy per ion and a 25% reduction of the expellant losses.

The results obtained in 1/2 to 1-1/2 hour runs are given in Table IV, together with the best performance measured with the life-test cathode in the same thruster. The results in Table IV indicate that thruster performance closely approximating the best obtained with low-temperature cathodes is now available with a cathode operating at the temperatures required for radiative heat rejection from the thruster shell, even when the thruster is part of an array.

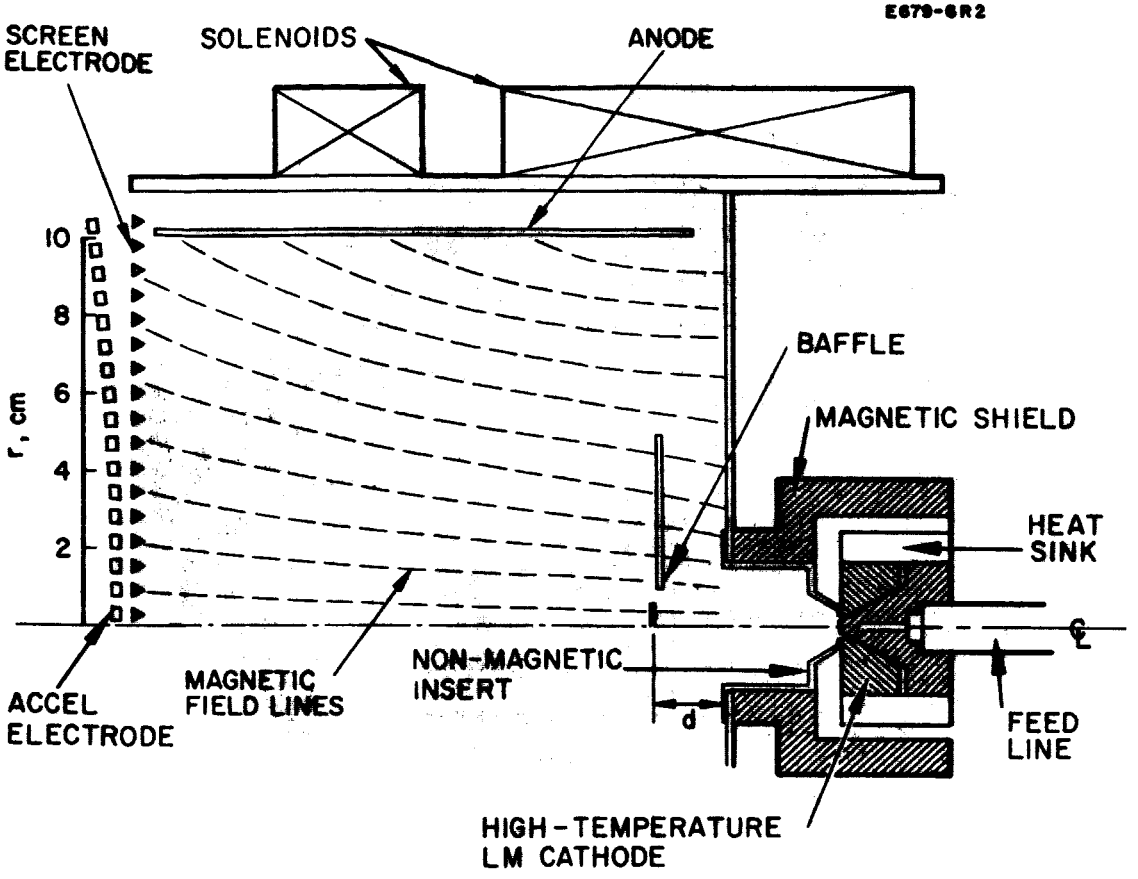

Fig. 25. Schematic cross section of 20-cm diameter electron-bombardment thruster with high-temperature LM cathode.

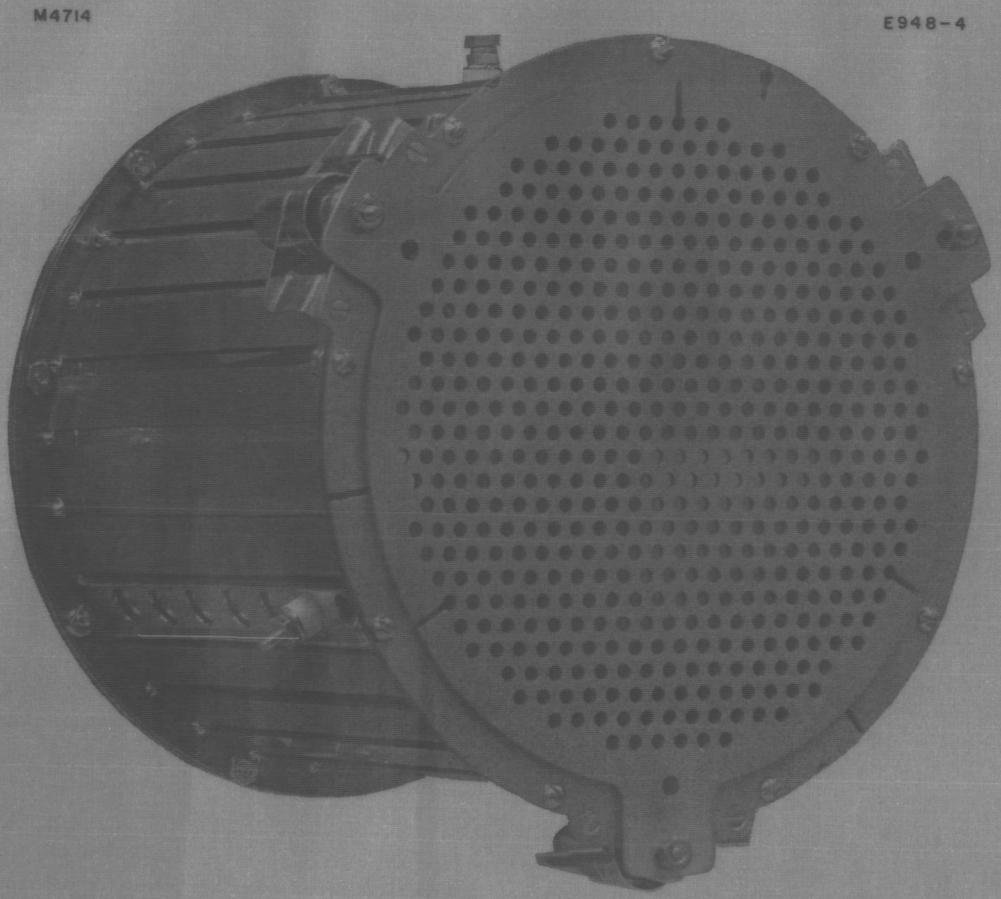

Fig. 26. Light-weight permanent magnet thruster.

TABLE IV

Results of Cathode Tests in 20-cm Thruster

Cathode Type	Cathode Temperature, °C	Mass Utilization, %	Source Energy[a] per Ion, eV/ion	Beam Current, mA	Cathode Current, A	K_e/K_a
Annular (No. 26)	250	87	400	680	7.6	9.8
	300	84	443	605	7.45	10.3
Circular (Life Test)	35	85	393	600	9	12.7

[a]Excluding magnet power (≈ 25 W).

2. Langmuir Probe Measurements

The 20-cm thruster was equipped with a heatable Langmuir probe and a two-dimensional probe movement mechanism. Figure 27(a) shows the probe mounted on a cathode feedthrough plate. The probe can be moved by the drive mechanism in both the axial and radial directions. The rod supporting the probe is 75 cm long and can traverse the entire length of the discharge chamber. The probe rotates about the axis of the rod in order to be able to sweep out all radial positions between the axis of the discharge chamber and a position of maximum excursion located at 80% of the anode radius.

Figure 27(b) shows the geometry of the probe tip. It consists of a hairpin loop of 0.003-in. diameter tungsten wire held at two points by an alumina insulator. Since the 0.010-in. separation between the adjacent segments of the hairpin loop is larger than a typical Debye length in the plasma under consideration, the two segments do not interact, and the hairpin configuration can be considered as a simple cylindrical probe of 0.003-in. diameter and 0.126 in. length.

Probe measurements were made in the vicinity of the circular life-test cathode in the 20-cm thruster under typical conditions of beam extraction. From these measurements conventional cold-probe Langmuir characteristics[10] of electron collection as a function of probe potential were obtained. The electron temperature was calculated from the slope of the electron-repelling region of the characteristic. The plasma density was then determined from the value of the electron saturation current, and the plasma potential was inferred from the location of the knee of the characteristic (i.e., the region of transition from the electron-repelling region to the electron-saturation region).

Since the Debye sheath is not much smaller than the probe diameter, the probe characteristic does not exhibit a very pronounced knee, nor is there a distinct saturation in the electron collection. Thus the values for plasma density and potential based on these features can only be considered as approximate. However, the curvature of the knee region provides information which permitted an alternative technique of data reduction using the Langmuir orbital analysis.[10] With this technique, the plasma density was obtained from measurements made in the vicinity of the knee alone. This value compared well with the value obtained by the electron saturation measurement. Since the value of the electron temperature (obtained from the electron-repelling region of the characteristic) was also known, the Langmuir orbital analysis permitted an accurate determination of the plasma potential from the cold probe data.

M5129

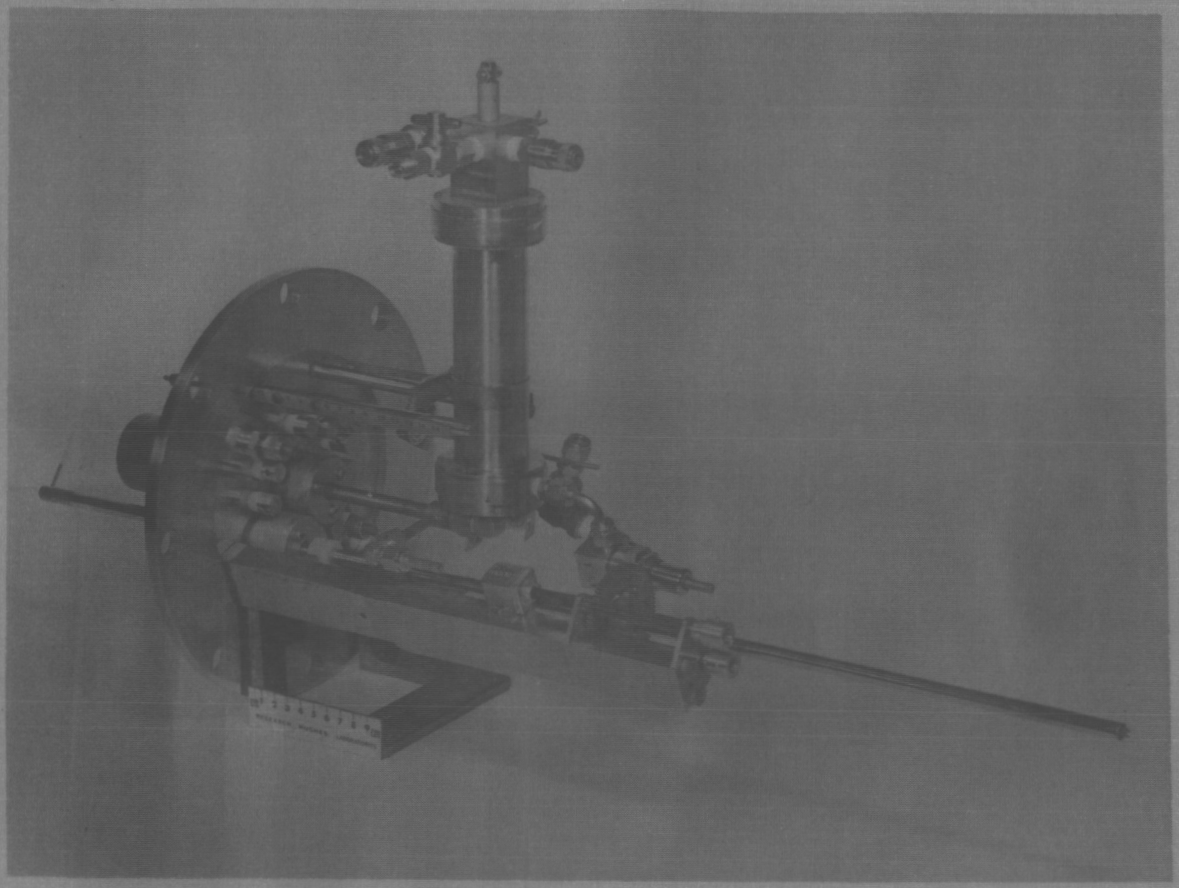

Fig. 27(a). Plasma probe installed on LM cathode feed-through plate.

E685-3

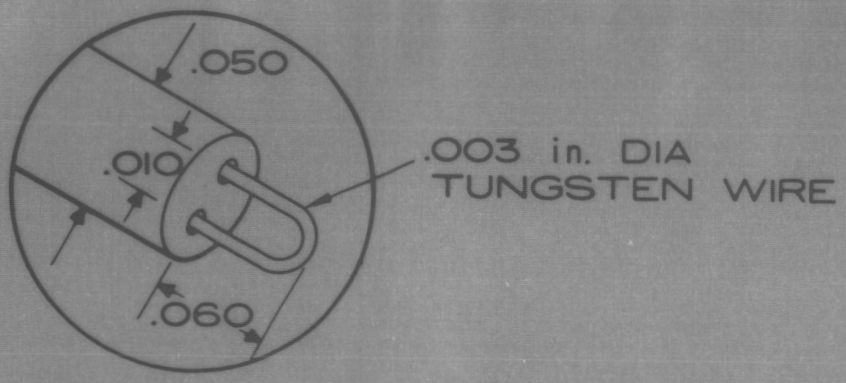

Fig. 27(b). Detail of probe tip.

The values of plasma potential obtained from the cold probe characteristic agree closely with those obtained from electron-emissive probe techniques.[11] This alternative technique utilizes the capability of this probe to be heated to electron-emissive temperatures. When the probe is held negative with respect to plasma potential, all electrons emitted by the probe are drawn into the plasma so long as this current is emission-limited to a value less than the double-sheath space-charge-limited value.[12] As the probe is made positive with respect to the plasma, there is an abrupt and easily observed decrease in electron current flowing from the probe which permits the value of plasma potential to be identified precisely.

From the measurements described above the electron temperature, plasma density, and plasma potential were determined as functions of position in the discharge chamber. Radial profiles of plasma density are shown in Fig. 28 and those of plasma potential are shown in Fig. 29, measured at three different axial positions in the vicinity of the cathode.

At a location 3.5 cm downstream of the cathode, 0.6 cm beyond the thruster end plate, the plasma density has a value of 7×10^{11} ion-pairs/cm^3 on the axis. It is highly peaked at the axis, decreasing radially with an initial e-folding distance of 1.1 cm. The plasma potential at this location is 10.7 V positive with respect to the cathode, a voltage difference slightly in excess of the ionization potential of mercury. The potential rises gradually with increasing radius, and close to the anode it reaches a maximum of a few volts above the anode potential of + 28 V.

Two centimeters forward, directly upstream of the baffle, the plasma description is virtually identical, except that the density has decreased by about 40%. In addition, the electron temperature, which is less than 2 eV closest to the cathode, increases to about 5 eV.

One-half centimeter farther forward, directly downstream of the baffle, the condition of the plasma changes abruptly. The plasma density is essentially constant at a value of 2.5×10^{11} ion pairs/cm^3 across a central region of 2 cm in diameter, peaking slightly in front of the annular aperture slot of the zone baffle plate at 1.8 cm diameter. Beyond the central region, the plasma density decreases radially with a radial e-folding distance of 2.5 cm. Downstream of the baffle the electron temperature measures 7.8 eV, and the plasma potential is everywhere slightly above anode potential, rising from 1.2 V above anode potential near the axis to a maximum in excess of 5 V above anode potential close to the anode.

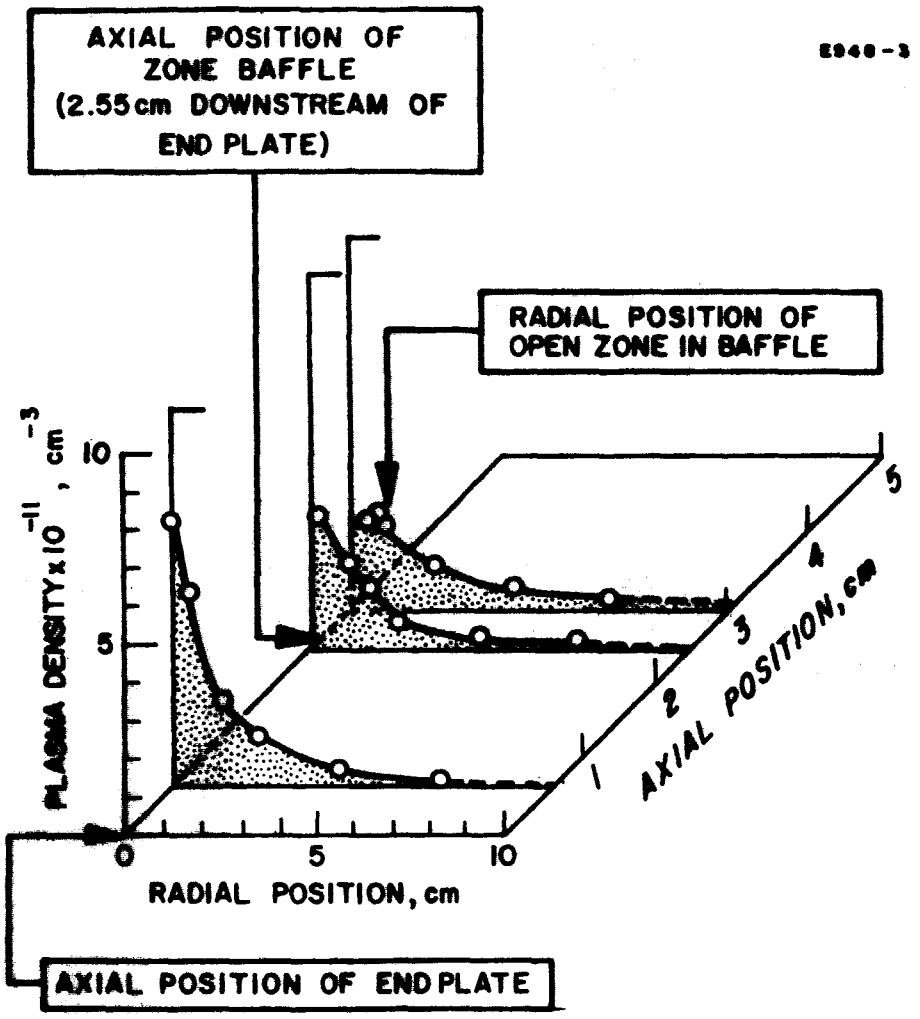

Fig. 28. Radial plasma density profiles for three axial positions.

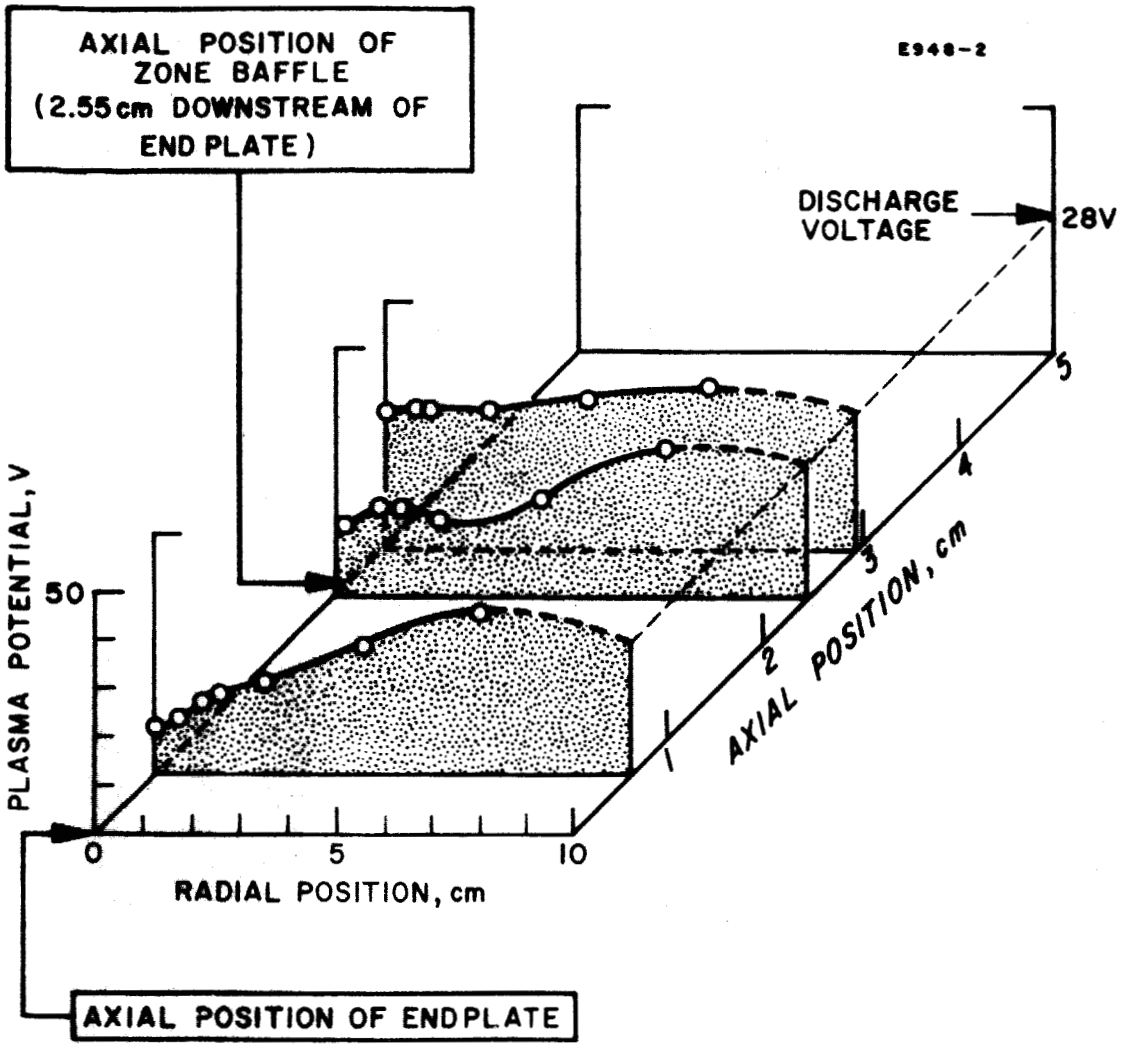

Fig. 29. Radial plasma potential profiles for three axial positions.

These measurements provide some insight into the mechanisms which prevail within the discharge, particularly with respect to the beneficial effects which result from use of the baffle. The plasma potential nearest to the LM cathode is as low as would appear possible for the maintenance of a "cold-cathode arc" discharge with a positive column (the electrons must at least be accelerated through a potential difference in excess of the ionization potential if they are to generate ions by impact). This indicates that the availability of electrons from the cathode is not limited by cathode saturation. The abrupt rise in plasma potential immediately downstream of the baffle clearly demonstrates one important function of this component. While still transmitting the copious supply of electrons generated by the cathode to the discharge region downstream, the baffle nevertheless provides sufficient isolation between these two regions to allow that part of the plasma where most of the extractable ions are generated to exist at a potential in excess of anode potential, thereby providing a condition by which the electrons are injected into the bulk of the discharge with a maximum initial energy. Furthermore, by reducing the gradients in plasma potential downstream, the baffle eliminates a potential trough which would otherwise accelerate ions toward the cathode. Finally, the baffle tends to reduce the radial drop-off in plasma density, thereby providing a more uniform ion arrival rate to the screen electrode for beam extraction.

C. 15-cm Diameter Thruster Experiments

1. Effect of Variable Aperture Baffle

Cathode No. 25 fitted with a variable aperture baffle was installed in the 15-cm diameter permanent-magnet geometry thruster. The baffle gave the choice of four central apertures of the following geometries:

a. circular, 1.9 cm diameter, 2.85 cm^2 open area

b. annular, 1.9 cm o.d., 1.32 cm^2 open area

c. annular, 1.9 cm o.d., 0.61 cm^2 open area

d. annular, 1.9 cm o.d., 0.28 cm^2 open area.

It was so designed that both the distance of the baffle from the cathode and the central aperture could be varied during thruster operation.

A series of experiments was performed to compare the thruster performance for the different configurations allowed by the four apertures and the variable axial baffle position. The axial position of the baffle was varied until the discharge was optimized for a particular central aperture. Table V lists the experimental results, which show that the best performance in terms of both the source energy per ion and the mass utilization was obtained with the smallest annular aperture, and with the baffle very close to the thruster end plate. (The significance of this result is discussed in Section IV-C-3.)

TABLE V

Experimental Results for Cathode No. 25
with Variable Aperture

Aperture	Aperture Area, cm^2	Source Energy/ Ion, eV/ion	Mass Utilization, η_m%	Distance of Baffle from Cathode Plate, cm
a	2.85	450	77.5	4.0
b	1.32	472	86.7	1.3
c	0.61	450	78.3	0.5
d	0.28	409	84	0.2

In subsequent experiments, the same cathode was operated with aperture d for continuous periods of up to 4 hours, while the cathode temperature at the thermocouple junction was maintained at 250°C. The average results are given in Table VI.

TABLE VI

Experimental Results for Cathode No. 25
using Baffle Aperture d

Cathode Temperature, °C	Mass Utilization, %	Source Energy/ Ion, eV/ion	Beam Current, mA	Cathode Current, A	K_e/K_a
250	80	400	440	7	13
250	82	417	440	5.9	11
250	88	426	490	7.2	13

They demonstrate satisfactory performance even though the outer diameter of the baffle had not been optimized for use with the 15-cm-diameter

2. Variation of the Discharge Voltage with Magnetic Field

While the 15-cm thruster was fitted with Cathode No. 25 and the variable four-aperture baffle, a plot was taken of the discharge voltage of the magnetic field at the midpoint of the thruster axis, for a constant discharge current of 7 A. The data (Fig. 30) show that for a given magnetic field, the aperture size has a strong effect on the discharge voltage; however, for optimum thruster performance (B ≈ 34G) the smallest aperture used requires just about the same discharge voltage as the other two annular apertures.

3. Probing-Baffle Experiments

The fact that the best thruster performance was obtained with a very small (but finite) annular baffle aperture has prompted us to replace the four-aperture baffle described in the previous section with a "probing" baffle, the latter having a small (0.6 mm diameter) pinhole and a narrow (0.25 mm width) slot which could be moved in turn over the central 1.9-cm diameter circular aperture. When the pinhole was displaced somewhat from the center of the baffle a slight peak was observed in the beam current I_B. The pinhole position for this peak corresponds closely with the optimum position of the annular baffle aperture described in Section IV-C-1. When the probing hole was moved to a larger radial position than the optimum one, the beam current fell rapidly to a "background" value which persisted even when the central hole in the main baffle was completely covered. The background I_B has been measured at less than 50% of the peak value of I_B, indicating that greater than 50% of the beam current production is caused by the flux of electrons and/or neutrals through the pinhole.

Assuming annular symmetry, the variation of I_B with slot position can also be used to check the result for the pinhole. Taking into account the geometrical effect as the slot is moved over the central hole, the incremental contribution to I_B can be found, and the results have been normalized to the pinhole values for comparison. Table VII shows that these normalized values show a dependence on radial position closely resembling that of the pinhole measurements.

We interpret these results as follows: The large effect on beam current of a small pinhole clearly proves that the proper distribution of the primary electrons within the discharge chamber is of utmost importance for the achievement of a high ion source efficiency. (This was already the guiding thought in the successful design of the zone baffle.) The primary electrons can escape easily from the dense plasma adjacent to the cathode into the main discharge chamber only if the baffle aperture is located within the boundary of this dense plasma. If the baffle aperture is made too large, not only electrons can escape, but

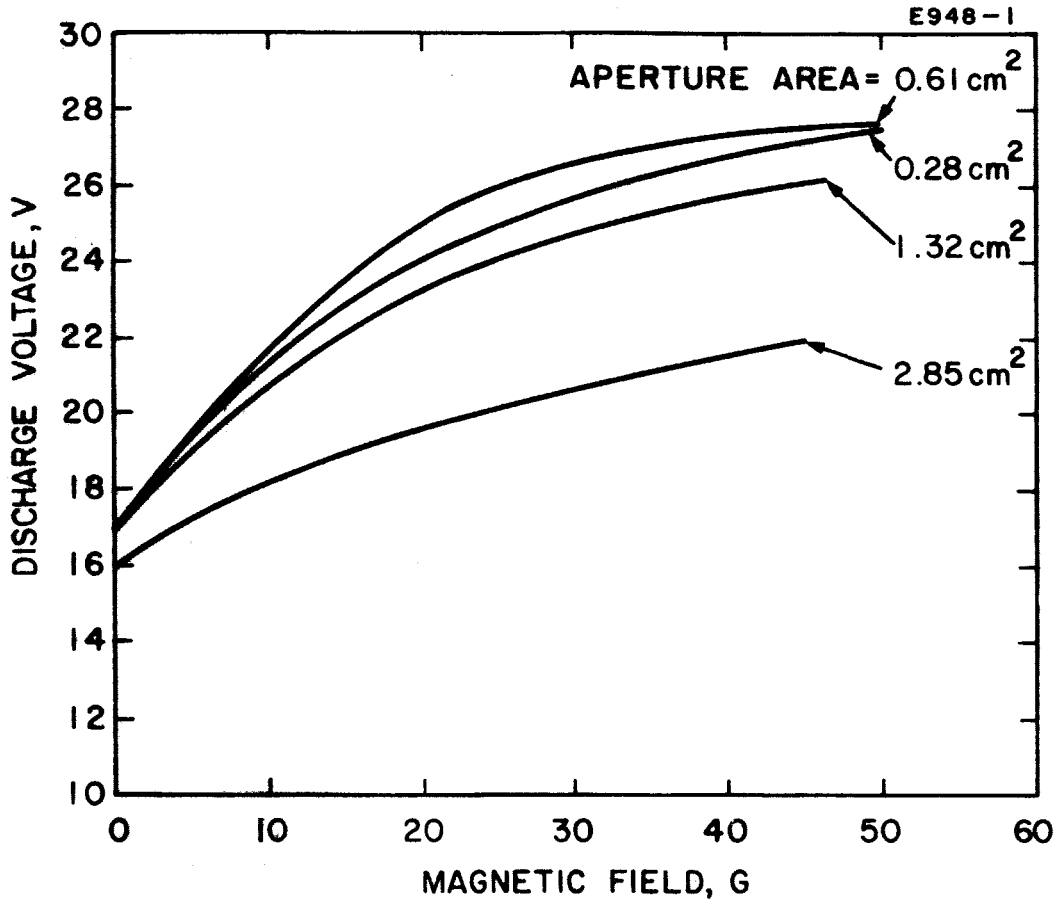

Fig. 30. Discharge voltage as a function of magnetic field for different aperture areas.

a sizable fraction of the neutrals emanating from the cathode can also enter the main discharge chamber without having first been distributed by multiple reflections; the results in Section IV-C-1 show that this is detrimental to ion source efficiency. The fact that optimum performance is obtained with a baffle aperture located near the boundary of the dense plasma region (as shown by the peak in beam current for an off-center pinhole position) suggests a nonuniform distribution of the electron density over the cross section of the dense plasma region.

TABLE VII

Dependence of Beam Current on Pinhole Position

Distance of Pinhole or Slot from Baffle Center, cm	I_B, mA (Measured for Pinhole)	I_B, mA (For Pinhole, Less "Background")	I_B, mA (For the Slot, Normalized, Less "Background")
0	400	200	200
0.24	420	220	218
0.48	440	240	300
0.72	350	150	75
0.96 (edge of central hole)	200	0	50
> 1.0	200 ("background")	—	—

In the same way that probe diagnostic measurements have provided insight into the effects of the zone baffle on the discharge mechanism, future probe analysis can be expected to increase our understanding of future diagnostic experiments involving baffles with movable apertures or apertures of variable size. As an outgrowth of such experiments, one may hope to affect relatively independently the admission of electrons and neutral atoms into the discharge chamber using improved versions of our discharge chamber baffles. This opportunity to separately optimize the admission of each species should lead to further substantial increases in thruster efficiency.

REFERENCES

1. H. R. Kaufman: "An Ion Rocket with an Electron-Bombardment Ion Source," NASA TN D585, January 1960.

2. W. O. Eckhardt, "Liquid-Metal Arc Cathode," patent applied for.

3. W. O. Eckhardt, J. A. Snyder, H. J. King, and R. C. Knechtli, "A New Cathode for Mercury Electron-Bombardment Thrusters," AIAA Paper No. 64-690, August 1964.

4. W. O. Eckhardt, H. J. King, J. A. Snyder, J. W. Ward, W. D. Myers, and R. C. Knechtli, "4000-hr Life Test of a Liquid-Mercury Cathode in a 20 cm LeRC Ion Thruster," Special Report, Contract NAS 3-6262, October 1966. H. J. King, W. O. Eckhardt, J. W. Ward, and R. C. Knechtli, "Electron-bombardment thrusters using liquid-mercury cathodes," J. Spacecraft and Rockets 4, 599 (1967).

5. W. O. Eckhardt, H. J. King, J. A. Snyder, and R. C. Knechtli, "Liquid-Metal Cathode Research," AIAA Paper No. 66-245, March 1966.

6. C. G. Smith, "Current densities of free-moving cathode spots on mercury," Brit. J. Appl. Phys. 4, 252 (1953).

7. K. G. Hernqvist, "Emission mechanism of cold-cathode arcs," Phys. Rev. 109, 636 (1958).

8. K. G. Hernqvist, "Hollow-cathode glow discharge in mercury vapor," RCA Review 19, 35-48 (1958).

9. W. O. Eckhardt, H. J. King, J. A. Snyder, J. W. Ward, G. Hagen, W. D. Myers, and R. C. Knechtli, "Liquid-Mercury Cathode Electron-Bombardment Ion Thrusters," Summary Report, Contract NAS 3-6262, October 1966.

10. F. F. Chen in Plasma Diagnostic Techniques, R. H. Huddlestone and S. L. Leonard, Eds. (Academic Press, New York, 1965).

11. R. F. Kemp and J. M. Sellen, "Plasma potential measurements by electron emissive probes," Rev. Sci. Instr. 37, 455 (1966).

12. D. Bohm in Characteristics of Electrical Discharges in Magnetic Fields, A. Gutherie and R. K. Wakerling, Eds. (McGraw-Hill, New York, 1949).

APPENDIX: INVENTIONS AND NEW TECHNOLOGY

A. Patentable Invention

During the investigations reported here, one invention which is believed to be patentable has been conceived and reduced to practice for the first time. The Patent Disclosure describing this invention has been forwarded to NASA Headquarters. The patent docket number, title, name of inventor, and date of first written description are as follows:

PD 67515 Vapor Feeding of LM Cathodes, by W.O. Eckhardt, March 1967.

B. New Technology

No new technologies have been developed in carrying out the experimental program described in this report.